# α-Phenylalanyl tRNA synthetase attenuates Notch signaling by competing with Notch through its N-terminal domain

Manh Tin Ho[1], Jiongming Lu[2], Beat Suter[1]

**Affiliations**:

[1]Institute of Cell Biology, University of Bern, Baltzerstrasse 4, Bern 3012, Switzerland.

[2]Present address: Max Planck Institute for Biology of Ageing, 50931 Köln, Germany.

Corresponding author: beat.suter@izb.unibe.ch

**Keywords**: aminoacyl tRNA synthetase, Su(H), Notch signaling, JAK/STAT signaling, stem cell, differentiation, proliferation, intestinal tumor

**Author contributions**: T.H., J.L., and B.S. conceived the ideas and designed the experiments. T.H. conducted most experiments and performed the analysis of the results. J.L. performed the loss-of-function experiments of PheRS and the mTOR signaling tests, the adult wing measurements and the FACS analysis, including analyzing their data. T.H., J.L., and B.S. wrote the manuscript.

# Summary

The alpha subunit of the cytoplasmic Phenylalanyl tRNA synthetase (α-PheRS) displays cell growth and proliferation activities and its elevated levels can induce cell fate changes and tumor-like phenotypes that do neither dependent on the canonical function of charging $tRNA^{Phe}$ with phenylalanine nor on stimulating general translation. In intestinal stem cells of Drosophila midguts, α-PheRS levels are naturally slightly elevated and in multiple human cancers the mRNA levels of the human homolog, *FARSA,* are also elevated. In the Drosophila midgut model, even moderately elevating α-PheRS levels caused the accumulation of many additional proliferating cells resembling intestinal stem cells (ISCs) and enteroblasts (EBs). This phenotype resembles the tumor-like phenotype described as *Notch* RNAi phenotype for the same cells. Genetic interactions between *α-PheRS* and *Notch* suggest that their activities neutralize each other and that elevated α-PheRS levels attenuate Notch signaling whether Notch induces differentiation into enterocytes, neuroblast stem cell proliferation, or transcription of a Notch reporter. These non-canonical functions all map to the N-terminal part of α-PheRS. An N-terminal α-PheRS polypeptide of approximately 200 amino acids (α-S) accumulates also naturally in the intestine and displays a weak sequence similarity to the Notch intracellular domain (NICD), suggesting that α-S competes with the NICD for binding to the BTD domain of the transcription factor Su(H)/CSL. Supporting this hypothesis, the key tryptophan (W) residue for this suggested interaction is not only conserved in α-PheRS and α-S, but also essential for attenuating Notch signaling.

53 # Introduction

54 Aminoacyl-tRNA synthetases (aaRSs) are essential enzymes that act by charging transfer
55 RNAs (tRNAs) with their cognate amino acid, a key process for protein synthesis (Schimmel
56 and Soll, 1979). Besides their well-known role in translation, aaRSs perform additional
57 functions in the cytoplasm, the nucleus, and even outside of the cell (Guo and Schimmel, 2013;
58 Nathanson and Deutscher, 2000; Smirnova et al., 2012) (Lee et al., 2004) (Casas-Tinto et al.,
59 2015; Gomard-Mennesson et al., 2007; Greenberg et al., 2008; Otani et al., 2002; Zhou et al.,
60 2014). Phenylalanyl-tRNA synthetase (PheRS, FARS, or FRS) displays elevated expression
61 levels in many cancers compared to their healthy counterparts according to the database "Gene
62 Expression across Normal and Tumor tissue" (GENT2; (Park et al., 2019)). Such a correlation
63 had been reported already two decades earlier and it was suggested that an alternative activity
64 of PheRS might contribute to the tumorigenic events (Sen et al., 1997) (Rodova et al., 1999).
65 A moonlighting function of the α subunit of Drosophila PheRS has recently been found to
66 promote growth and proliferation in different tissues (Ho et al., 2020). Despite this, a possible
67 mechanism explaining the connection between elevated PheRS levels and tumor formation had
68 so far not been reported and, to our knowledge, also not been studied.

69 Cytoplasmic PheRS is the most complex member of the aaRSs family, a
70 heterotetrameric protein consisting of 2 alpha- (α) and 2 beta- (β) subunits responsible for
71 charging $tRNA^{Phe}$ for translation (Roy and Ibba, 2006). The α subunit includes the catalytic
72 core of the tRNA synthetase and the β subunit has structural modules with a wide range of
73 functions, including tRNA anticodon binding, hydrolyzing misactivated amino acids, and
74 editing misaminoacylated $tRNA^{Phe}$ species (Ling et al., 2007; Lu et al., 2014; Roy and Ibba,
75 2006). Importantly, both subunits are needed for aminoacylation of $tRNA^{Phe}$.

76 We set out to address the question of whether and how the elevated levels of α–PheRS
77 that induce growth and proliferation (Ho *et al.*, 2020) might contribute to tumor formation. To
78 test for this activity, we studied the role of α–PheRS levels in the Drosophila model system to
79 dissect the molecular mechanism of such a moonlighting role of *α–PheRS.* Tissue growth and
80 homeostasis play important roles in developing and outgrown animals, and they require tight
81 control of stem cell self-renewal and differentiation into daughter cells. The Drosophila midgut
82 is a powerful model to analyze these mechanisms and their interplay. Adult intestinal stem cells
83 (ISCs) and adult midgut progenitors (AMPs) in the larval gut can either divide asymmetrically
84 or symmetrically (Jiang and Edgar, 2011; Micchelli, 2012). Asymmetric divisions of ISCs give
85 rise to a new ISC and a Su(H)GBE$^{+}$ enteroblast (EB) for the enterocyte (EC) lineage
86 differentiation, or a pre-enteroendocrine cell (pre-EE) for the enteroendocrine (EE) cell lineage
87 differentiation (Furriols and Bray, 2001; Guo et al., 2016). Differential Delta/Notch signaling
88 between the ISC and its daughter causes the latter to either differentiate into an absorptive EC
89 lineage or a secretory EE lineage by distinct mechanisms (Beehler-Evans and Micchelli, 2015;
90 Micchelli and Perrimon, 2006; Ohlstein and Spradling, 2007; Zeng and Hou, 2015). EBs are
91 intermediate differentiating cells that differentiate into ECs in a Notch-dependent manner
92 (Ohlstein and Spradling, 2006), while the production of EEs has not been molecularly
93 characterized. However, the pre-EEs require only low levels of Notch signaling to differentiate
94 into EEs (Guo *et al.*, 2016). Intestinal homeostasis is an interesting system to elucidate the
95 control of continuous replenishment of lost cells and the maintenance of stem cells.
96 Additionally, it turned out to be also a very dynamic process that can react to the loss of large
97 numbers of differentiated cells in response to injuries and bacterial infections.

98 We found that in different tissues and cell types, α-PheRS levels in stem and progenitor
99 cells regulate cell proliferation, cell differentiation, or both. Interestingly, a proteolytic α-
100 PheRS fragment that can neither interact with β-PheRS nor perform aminoacylation, promotes

101 these growth, proliferation, and differentiation functions. Although the consequences of altered
102 levels vary to some degree between tissues, we found that even in tissues with the most
103 divergent consequences, α-PheRS levels act by attenuating Notch signaling. Sequence analysis
104 combined with genetic and biochemical tests points to a mechanism whereby the N-terminal
105 "DNA binding domain" of α-PheRS competes with the NICD for the binding to the
106 transcription factor Su(H)/CSL. Such a regulative mechanism can explain all moonlighting
107 activities of α-PheRS described here.

108 # Results

109 **PheRS is enriched in Drosophila gut stem cells**

110 PheRS promotes growth and proliferation in different tissues (Ho *et al.*, 2020). In the
111 Drosophila midgut, intestinal stem cells (ISCs) display very high proliferation rates (Nagy et
112 al., 2018) due to a high turnover of the cells with a nutrient absorption mission. In addition, the
113 GENT2 database also reports highly elevated PheRS levels in many malignant cells compared
114 to normal tissues, and among these are also intestinal cancers (Park *et al.*, 2019). To investigate
115 the role of PheRS in intestinal cells, we examined the PheRS expression levels in wild-type fly
116 guts. ISCs and AMPs are ideal to study the novel PheRS activity because they can both undergo
117 either symmetric or asymmetric divisions and differentiate to maintain the cell population in
118 the fly gut. We observed that adult midguts express naturally elevated levels of α-PheRS in the
119 diploid wild-type ISC/EB cells compared to the enterocytes in the same tissue (Fig 1 A-A", B).
120 Similarly, a Myc-tagged α-PheRS under the normal genomic *α-PheRS* promoter is expressed
121 at higher levels AMPs than in enterocytes of larval guts (Fig 1 C-C", D). Therefore, α-PheRS
122 levels are generally higher in midgut progenitors than in differentiated cells of this tissue.

123

124 **Elevated α-PheRS levels promote ISC and EE accumulation and altered EB morphology**

125 We previously constructed a mutant *α-PheRS* gene, that encodes an aminoacylation-dead
126 subunit (*α-PheRS*$^{Cys}$) that still displays the non-canonical activity of promoting growth and
127 proliferation (Ho *et al.*, 2020). This mutant allows us to specifically study the activities of *α-*
128 *PheRS* that are not dependent on the aminoacyl tRNA synthetase activity of PheRS. To
129 investigate the effect of elevated levels of α-PheRS and α-PheRS$^{Cys}$ (α-PheRS$^{(Cys)}$) on adult
130 midgut ISCs and EBs, we used *α-PheRS*$^{(Cys)}$ under UAS control together with the *esg-*
131 *Gal4*, *tub-Gal80*$^{ts}$, *UAS-2XeYFP* system (Micchelli and Perrimon, 2006). In the following text,

132 we will refer to this as the *esg*$^{ts}$ driver or system. The *esg*$^{ts}$ driver induces a specific and
133 conditional activation of *α-PheRS*$^{(Cys)}$ expression in ISCs and EBs once the temperature is
134 shifted to 29ºC. Co-expression of *UAS-2XEYFP* allowed us to monitor the activity of the *esg-*
135 *Gal4* driver and to label ISCs and EBs. Upon controlled upregulation of α-PheRS$^{(Cys)}$ levels,
136 we observed two cellular changes in the intestines as early as 2 days after induction and the
137 phenotypes became more pronounced until day 5 (Fig 1E). The first phenotype was a *Notch*
138 (*N*) knockdown-like phenotype with a 4.3 and 4.7 fold, respectively, increase of the total
139 numbers of YFP$^{+}$ cells upon additional expression of α-PheRS and α-PheRS$^{Cys}$, respectively
140 (Fig 2A-C"', G). The increase of these midgut progenitor cells (ISCs and EBs) could be a
141 consequence of a differentiation problem of ISCs (Lian et al., 2018; Mundorf et al., 2019).
142 Indeed, we also observed an increase in the proportion of EEs from 8% in the control to 12%
143 in the posterior midguts with elevated *α-PheRS* expression (Fig 2H), indicating that elevated
144 expression of *α-PheRS* promotes ISC proliferation and EE accumulation.

145 The controlled upregulation of *α-PheRS*$^{(Cys)}$ levels also led to a second phenotype, an
146 altered morphology of EBs. We observed a hyperaccumulation of YFP$^{+}$ polyploid cells that
147 resembled the ones that have been referred to in other studies as "differentiating" EBs (Loza-
148 Coll et al., 2014; Zhai et al., 2017). Because these cells express ISC/EB characteristics (YFP$^{+}$)
149 and EC characteristics (polyploid) at the same time, it appears that they arrested development
150 between these two fates. Differentiating EBs were rarely observed in wild-type midguts (3%
151 of progenitor cells; Fig 2A-A"', I) and if they were present, they retained only weak YFP
152 signals. In midguts expressing elevated levels of α-PheRS$^{(Cys)}$, we observed much higher levels
153 of "differentiating" EBs (20% and 22%, respectively, of the YFP$^{+}$ progenitor cells), and these
154 cells also displayed a strong YFP signal (Fig 2B-C"', I). We concluded that the elevated levels
155 of α-PheRS in the intestine induce hyperaccumulation of ISCs and EEs, and alterations in EB
156 morphology.

157

158 **Similarities between elevated α-PheRS levels and low Notch activity**

159 Notch signaling is an important signaling pathway that coordinates ISC proliferation and
160 differentiation (Ohlstein and Spradling, 2006) and the above-described changes regarding ISCs
161 and EEs were very similar to the low *N* activity phenotype that had been reported in several
162 studies (Guo and Ohlstein, 2015; Liu et al., 2010; Marianes and Spradling, 2013; Micchelli and
163 Perrimon, 2006; Ohlstein and Spradling, 2007). To confirm this similarity, we knocked down
164 *N* with RNAi treatment with the same $esg^{ts}$ system and this, indeed, led to a similar phenotype
165 in ISC proliferation and EE accumulation as elevated *α-PheRS*$^{(Cys)}$ levels did. The increase in
166 $YFP^{+}$ cells (290%; from 27 to 104 cells) was similar to the one observed under elevated *α-*
167 *PheRS* expression (332%; from 27 to 115 cells), and with 12%, the proportion of EEs was the
168 same under the two conditions (Fig 2D-D"', G, H). In contrast, using the $esg^{ts}$ driver in wild-
169 type adult midguts to upregulate Notch signaling by expressing the continuously active form
170 of Notch, the Notch intracellular domain (NICD), drives ISCs to differentiate into ECs, thereby
171 depleting 80% of the ISC pool (Fig 2E-E"', G) and inhibiting EE differentiation (Fig 2E-E"',
172 H) as it has been reported in previous studies (Micchelli and Perrimon, 2006; Zhai *et al.*, 2017).

173 To test whether α-PheRS$^{(Cys)}$ interferes with Notch signaling, we simultaneously
174 elevated levels of *α-PheR*S$^{(Cys)}$ and NICD. This schema had a rescuing effect on both
175 phenotypes. On the one hand, it rescued the ISC pool and proportion of EEs depleted by NICD
176 expression even beyond the wild-type levels (Fig 2F-F"', G). On the other hand, the phenotype
177 caused by the additional expression of the NICD can also be interpreted as a partial rescue of
178 the phenotype caused by elevated α-PheRS$^{(Cys)}$ levels. The numbers of $YFP^{+}$ cells and
179 differentiating EBs dropped considerably, even though they remained still higher than in the
180 wild type (Fig 2D-F"', G, I). These results suggest that the two phenotypes observed when *α-*

181 *PheRS*$^{(Cys)}$ expression was elevated in ISCs and EBs arise because *α-PheRS*$^{(Cys)}$ and Notch
182 signaling counteract each other for the control of proliferation and differentiation. They might
183 for instance either neutralize each other or compete for common downstream targets.

184

185 **Elevated α-PheRS levels induce AMP proliferation and interfere with gut homeostasis**

186 Larval Drosophila midguts possess AMPs as the temporary reserve for adult ISCs. AMPs go
187 through several divisions to form imaginal midgut islets that include AMPs enclosed by a
188 peripheral cell (PC) (Mathur et al., 2010). Due to the transient period of the larval stage, larval
189 midguts do not require EC renewal under normal conditions (Lee and Lee, 2019). However,
190 Houtz et al. reported recently that larval guts can respond to certain damages and injuries by
191 triggering a regenerative process that compensates for depleted ECs in the epithelium and also
192 allows reconstituting the AMP pool (Houtz et al., 2019). We investigated the effect of elevated
193 *α-PheRS* levels on larval AMPs by using the *esg-Gal4, UAS-2XEYFP* driver, which is
194 specifically expressed in AMPs. Co-expression of *UAS-2XEYFP* allowed us to monitor the
195 activity of the *esg-Gal4* driver and to label AMPs. The results demonstrated that elevated
196 Myc::α-PheRS in the larval midgut significantly increased the proportion of PH3 positive cells
197 (mitotic index) in the posterior midgut (Fig 3A-B', E-E", F). Driving the expression of the α-
198 PheRS$^{Cys}$ mutant in AMPs also produced a higher mitotic index (Fig 3C-C', F), indicating that
199 the aminoacylation function is not required for this activity. Due to the lack of epithelial
200 renewal in normal larval guts, the cell density of larval midguts is usually stable (Lee and Lee,
201 2019; Mathur *et al.*, 2010). It is therefore surprising that elevated α-PheRS$^{(Cys)}$ levels increase
202 the cell density in larval midguts (Fig 3G). Altogether, these results show that elevated α-
203 PheRS$^{(Cys)}$ levels cause AMPs to proliferate and to differentiate, producing additional larval
204 midgut cells.

205 Strikingly, elevated α-PheRS$^{Cys}$ levels induced tumor-like phenotypes in both anterior
206 and posterior areas of the larval midgut (outlined with white dashed lines, Fig 3C-C') while the
207 elevation of wild-type Myc::α-PheRS only gave rise to high numbers of AMPs in the posterior
208 larval midgut (Fig 3B-B'). Interestingly, elevated α-PheRS$^{Cys}$ levels also caused the
209 appearance of a more severe tumor-like phenotype, where individual AMP islets could not be
210 discerned anymore (Fig 3C-C'). Wild-type larval guts contain ECs with large nuclei and
211 interspersed occasional AMP islets with smaller nuclei (as seen in the YFP overexpression
212 control, Fig 3A-A'). In contrast, we observed a phenotype where ECs and AMPs could not be
213 distinguished based on the size of their nuclei but emerged as a larger cell population with
214 intermediate size nuclei (Fig 3C'). Many of these cells expressed the *esg*>YFP stem cell marker
215 at high levels, but others displayed only a very weak YFP signal. This result is comparable to
216 the EB phenotype in adult midguts where the progenitor cells remain in an intermediate
217 differentiation state (Fig 2 B''', C'''). Notably, this phenotype was also observed when Notch
218 was downregulated by RNAi using the same induction system (Fig 3D-D').

219 We next tested whether α-PheRS$^{(Cys)}$ is able to downregulate *Notch* signaling in adult
220 midguts using the *Notch* reporter NRE-eGFP (Notch response element promoter driving the
221 expression of eGFP; (Saj et al., 2010)). As seen in Fig 3H, the expression of either of them
222 clearly reduced the *N*-driven expression of the N-signaling reporter. We concluded that
223 elevated α-PheRS levels in midgut stem cells cause misregulation of gut homeostasis, possibly
224 by downregulating Notch signaling and inhibiting the terminal differentiation of the progenitor
225 cells (EBs).

226

227 ***α-PheRS* is a novel general repressor of Notch signaling**

228 Developing larval brains contain neuroblasts (NBs), neuronal stem cells that divide
229 asymmetrically with one daughter keeping the stemness and the other differentiating into a
230 neuronal cell. Notch signaling plays a crucial role in this process (Ables et al., 2011; Giachino
231 and Taylor, 2014), but in contrast to the situation in the gut, loss of *Notch* prevents NB self-
232 renewal, whereas ectopic expression of activated Notch leads to tumor formation (de la Pompa
233 et al., 1997; Grandbarbe et al., 2003; Hatakeyama et al., 2004). This opposite role of *Notch*
234 makes the NB lineage an ideal complementary system to test whether α-PheRS is a general
235 component of the *Notch* pathway. Driving α-PheRS or the α-PheRS$^{Cys}$ expression in NBs with
236 the *inscutable-Gal4 (incs-Gal4)* driver resulted in significantly smaller central brains (CB), the
237 region where the Type I and II NBs are located (Fig 4A-A'', B). In contrast, this treatment had
238 little or no effect on the size of the optic lobes (OL). Importantly, the phenotype was virtually
239 indistinguishable from the phenotype caused by *N* knock-down, although the phenotype of the
240 latter might show slightly higher expressivity. Analogous to the situation in the gut, co-
241 expression of NICD together with *α-PheRS$^{Cys}$* in neuroblasts rescued the brains to wild-type
242 size (Fig 4B).

243 Type II neuroblasts are particularly suited to analyze effects on neuroblast
244 differentiation. Targeting specifically the 8 type II neuroblasts in central brain lobes with *α-*
245 *PheRS* or *α-PheRS$^{Cys,}$* overexpression, resulted in half of the central brains in a strong reduction
246 of the number of neuroblasts, and the resulting central brain lobes ended up smaller (Fig 4C-F,
247 I). Knocking down *Notch* in type II NBs with RNAi and the same driver combination resulted
248 in a similar phenotype, but with a higher expressivity (Fig 4F). On the other hand,
249 overexpression of α-PheRS in type II neuroblasts where Notch signaling was also over-
250 activated by the co-expression of NICD and α-PheRS, partially rescued the tumor phenotype
251 of type II neuroblasts to wild-type numbers and it restored the normal size of the brain (Fig

252 4G). Because the genetic interaction with *Notch* shows that the two activities counteract one
253 another in guts and brains, two tissues where *Notch* has opposing functions on cellular
254 differentiation, it appears that the interaction between *α-PheRS* and *Notch* is not mediated
255 indirectly through a primary effect on division or differentiation but is likely to be a more direct
256 one. In any case, this interaction appears to modulate tissue homeostasis in different organs.

257 To further address the role of *α-PheRS* on Notch signaling, we also studied its effect on
258 the larval wing disc and the adult wing. Using the *en-Gal4*, *tub-Gal80*$^{ts}$ (referred to as *en*$^{ts}$
259 system) to elevate *α-PheRS* expression allowed us to specifically and conditionally activate *α-*
260 *PheRS*$^{(Cys)}$ expression in the posterior compartment of the wing disc by temperature-shift
261 control. Reduced Notch signaling in the posterior wing disc can cause the notched wing
262 phenotype at the distal end of the wing and the emergence of an ectopic partial vein in the
263 center of the posterior compartment. The additional expression of *α-PheRS*$^{(Cys)}$ in the posterior
264 compartment did not produce the distal phenotype and we will discuss possible reasons for this
265 in the Discussion. However, elevated *α-PheRS* or *α-PheRS*$^{Cys}$ levels induced the central ectopic
266 vein phenotype also observed under low Notch signaling conditions (Fig 5A; (Johannes and
267 Preiss, 2002). The new vein branches off from the connecting vein between the L4 and L5 vein
268 (arrowhead, Fig 5A', A") and is indistinguishable from the one obtained by downregulating
269 *Notch* by RNAi treatment using the same expression system (Fig 5A"'). Again, these findings
270 suggest that *α-PheRS* might be a more general, novel regulator of Notch signaling.

271 To test directly for changes in *Notch* activity in response to altered levels of *α-*
272 *PheRS*$^{(Cys)}$ in imaginal wing discs, we monitor Notch activity with the NRE-eGFP reporter and
273 used the *en*$^{ts}$ system together with *UAS-mRFP* to conditionally express *α-PheRS*$^{(Cys)}$ in the
274 posterior compartment. In this system, *eGFP* expression marks the cells with active Notch
275 signaling, which normally happens along the dorsal-ventral (D/V) boundary of the larval wing
276 disc (Fig 5B"), and it marks the posterior, en-Gal4$^{+}$, compartment of the wing disc with mRFP,

277 allowing us to assess *N* activity in this compartment (black arrowhead, Fig 5B”’) while using
278 the anterior compartment as the internal control. In wild-type wing discs, the NRE-eGFP signal
279 is as strong in the posterior compartment as in the anterior one (Fig 5C-C”’). Knockdown of
280 *Notch* in the posterior compartment resulted in the exclusion of the NRE-eGFP signal from the
281 mRFP-marked posterior compartment (white arrow, Fig 5F-F”’). Importantly, elevated *α-*
282 *PheRS*$^{(Cys)}$ levels also caused a loss of eGFP signal in the mRFP-marked posterior
283 compartments (Fig 5D-D”’, E-E”’). These observations demonstrate that elevated *α-PheRS*
284 levels downregulate *Notch* activity in larval wing discs. Taken together, the results from
285 midguts, brains, and wing discs demonstrate that *α-PheRS* is a novel general repressor of *Notch*
286 signaling.

287

288 **The N-terminal 200 amino acids of α-PheRS (α-S) are sufficient to repress Notch activity**

289 Having shown that the growth and proliferation function and the counteracting of the Notch
290 signaling are independent of the aminoacylation activity of α-PheRS, we wanted to find out
291 whether this activity can be separated from the catalytic domain. As shown in Fig 6A,B, the C-
292 terminal catalytic domain is separated by a linker region from the N-terminal part. We,
293 therefore, cloned the first 200 codons of the α-PheRS ORF under UAS control and added a
294 Myc tag at its N-term, giving rise to the *Myc::α-S* (*α-S*) gene (Fig 6B). To test whether this C-
295 terminally truncated isoform was able to repress Notch signaling, too, we expressed *α-S* with
296 the esg$^{ts}$ driver in larval and adult guts and found that it produced an excessive number of Esg$^{+}$
297 cells (Fig 6C-C”’, D-D”’), an increase in mitotic cells (Fig 6F), and that it diverted ISC
298 differentiation toward the EE fate (Fig 6E, E’, G). Evidently, this truncated isoform, α-S, is
299 capable of inducing the production of many cells with stem cell characteristics and it directs
300 their differentiation towards an EE fate, just like α-PheRS$^{(Cys)}$ does. Similarly, expressing *α-S*
301 in the posterior compartment of wing discs induced the ectopic vein formation between the L4

302 and L5 veins in the adult wing (black arrowhead, Fig 6H-H'). Additionally, this *α-S* expression
303 caused the same loss of the Notch reporter signal (NRE-eGFP) in the posterior compartments
304 of wing discs as full-length *α-PheRS*$^{(Cys)}$ did (Fig 6I-J'). These observations demonstrated that
305 elevated *α-S* levels downregulate *Notch* and that the α-S polypeptide sequence contains the
306 inhibitory activity of *α-PheRS* on Notch signaling.

307 Expressing transgenic Myc::α-PheRS under the control of the *Tub-Gal4* driver revealed
308 beside the full-length α-PheRS isoform (55kDa) also one stable isoform around 40 KDa and
309 another around 25KDa (Fig 6K). To study the expression pattern of these isoforms, we
310 dissected different larval tissues and found that the 40 KDa isoform was present in larval heads
311 and fat bodies, while larval guts showed predominantly the 25 KDa isoform (Fig 6L). The 25
312 KDa isoform might either arise if Myc::α-PheRS is cleaved in the linker domain or if the pre-
313 mRNA is processed in a different way to give rise to a shorter, but stable isoform. Because
314 there is no evidence for alternatively processed mRNAs of α-PheRS in wild-type animals
315 (flybase.org version FB2019_04; (Thurmond et al., 2019), we tested whether PheRS might get
316 cleaved *in vivo* to produce an isoform that resembles Myc::α-S. Myc-tagged isoforms were
317 isolated from total larvae by immunoprecipitation and gel purification, and their polypeptides
318 were identified by mass spectrometry (MS). The MS data shows the peptide coverage of the
319 25KDa isoform according to the score of Peptide Spectrum Matches (PSM; Fig S1). The 25
320 KDa isoform contains the peptides of the N-terminal 28% of the full-length α-PheRS. Even
321 though we identified two more C-terminal peptides, which could not be rejected based on the
322 PSM interpretations, these two peptides were likely recovered due to a "memory effect" of the
323 column. This indicates that the 25 KDa isoform is a C-terminally truncated version of α-PheRS
324 that strongly resembles the α-S that performs the non-canonical functions.

325

326

327 **Mechanism of downregulating Notch signaling by α-S**

328 Given the competitive interaction between *α-PheRS* and *Notch* and the effect of the α-S isoform
329 on downregulating N activity, we aligned the polypeptide sequence of α-S and Notch, and this
330 revealed similarities between α-S and the RAM domain (RBP-Jκ-associated molecule) of
331 Notch (Fig 7A). To transmit the Notch activity, the RAM domain of the NICD binds through
332 the tetra-peptide motif ΦWΦP to the beta-trefoil domain (BTD) of Suppressor of Hairless
333 (Su(H)), the Drosophila CSL/RBPJ. This allows the complex to interact with specific DNA
334 sequences in the promoter region of the target genes to activate transcription (Barrick and
335 Kopan, 2006; Borggrefe and Oswald, 2009; 2016; Gordon et al., 2008; Kovall, 2007).
336 Mammals can repress Notch activity with proteins containing the tetra-peptide motif ΦWΦP.
337 These compete with NICD to bind to CSL/RBPJ and form the Complex of Repressor (CoR)
338 that inhibits Notch target gene activation (Bray and Furriols, 2001; Fortini and Artavanis-
339 Tsakonas, 1994; Nagel et al., 2017; Praxenthaler et al., 2017). Even though the tetrapeptide is
340 only partially conserved in α-S, the similarities between α-S and the RAM domain of Notch,
341 and the presence of the tryptophan residue (W) flanked by Φ (Fig 7A) led us to hypothesize
342 that α-S and NICD compete for binding to Su(H) to downregulate Notch activity.

343 To test this hypothesis, we mutated the conserved "W" (tryptophane) codon in *α-S*
344 (*Myc::α-S*$^{W112A}$) and analyzed the effect of this mutation on Notch signaling. As opposed to the
345 wild-type version, expressing *Myc::α-S*$^{W112A}$ with the *esg*$^{ts}$ driver in adult guts did not induce
346 the proliferation phenotypes, such as excessive numbers of Esg$^{+}$ cells and EE fate changes as
347 the wild-type *α-PheRS* did (Fig 7B, C, G, H). These results could also be confirmed when a
348 full-length version of *α-PheRS* with the mutation W112A was expressed with the same driver
349 (Fig 7D, G, H). To further test whether α-PheRS with the W112A mutation lost its ability to
350 interfere with Notch signaling, we simultaneously elevated levels of Myc::α-S$^{W112A}$ or α-
351 PheRS$^{W112A}$ together with NICD levels. Indeed, the mutated Myc::α-S$^{W112A}$ or α-PheRS$^{W112A}$

352 did not rescue the ISC pool or the EEs, the two cell types that are depleted by NICD over-
353 expression (Fig 7F-F"', G, H). Furthermore, because a genomic construct expressing this
354 mutant version of *α-PheRS*$^{W112A}$ *(gα-PheRS*$^{W112A}$*)* under its native promoter rescued the *α-*
355 *PheRS* null mutant, the W112A mutation does not prevent the canonical activity of *α-PheRS*
356 and produces sufficient protein that can perform the aminoacylation reaction. These results,
357 therefore, show that $W^{112}$ in *α-PheRS* plays an important role in counteracting Notch signaling
358 in ISCs and EBs and they suggest a mechanism by which *α-PheRS* acts to attenuate Notch
359 signaling. It seems to compete with the RAM domain of NICD for the binding to the
360 downstream target, the transcription factor of the Notch pathway.

361

362 # Discussion

363 Notch signaling regulates diverse cellular behaviors during tissue growth in a context-
364 dependent manner. Most prominently, these are proliferation and differentiation (Henrique and
365 Schweisguth, 2019; Hori et al., 2013). In this study, we presented the effect of α-PheRS on
366 downregulating Notch signaling activity in different tissues where Notch induces diverse
367 outcomes. In the larval brain, Notch signaling promotes NB self-renewal, and ectopic
368 expression of NICD leads to tumor formation (de la Pompa *et al.*, 1997; Grandbarbe *et al.*,
369 2003; Hatakeyama *et al.*, 2004). Here, elevated α-PheRS showed an inhibitory effect on Notch
370 signaling, preventing NB self-renewal and thereby reducing the size of the brain lobe (Fig 4A-
371 A",B). Accordingly, elevated α-PheRS in this situation also rescued the tumor phenotype
372 caused by the expression of the activated form of Notch, NICD (Fig 3 G,H). Also in this
373 situation, expressing only the N-terminal part of α-PheRS, the region that does not contain any
374 catalytical domains and that does not interact with the β-PheRS subunit (Fig 6C; (Finarov et
375 al., 2010)) was just as effective in producing the same phenotypes as α-PheRS$^{(Cys)}$.

376 Elevated levels of α-PheRS reproduced the "vein formation" phenotype in the adult
377 wings caused by loss-of-Notch (Fig 6A-A"') (Johannes and Preiss, 2002) and its elevated levels
378 also downregulated Notch activity at the D/V boundary in larval wing discs (Fig 6D-E"').
379 Reminiscent of its function in neuroblasts, Notch signaling at the D/V boundary region of the
380 wing disc promotes proliferation (de Celis et al., 1996). Upon additional expression of α-
381 PheRS in this region, not only Notch activity (Fig 5), but also PH3$^{+}$ cells became absent from
382 this region (Ho *et al.*, 2020). Interestingly, however, in regions of the posterior wing disc
383 compartment where there is no Notch activity, elevated α-PheRS caused the appearance of
384 additional pH3$^{+}$ cells (Ho *et al.*, 2020). Because knockdown of *N* causes the notched wing
385 phenotype but increased α-PheRS levels do not (Fig 6A), it would be interesting to find out

386 whether the proliferation of these additional pH3$^{+}$ cells that reside outside of the region with
387 *Notch* activity can compensate for the cells along the D/V boundary that depend on Notch
388 signaling to be mitotically active. Moreover, cell proliferation in the distal wing margin is
389 regulated not only by Notch signaling but also by epidermal growth factor (EGF) or
390 decapentaplegic (Dpp)/bone morphogenetic protein (BMP) signaling (Biehs et al., 1998;
391 Teleman and Cohen, 2000). While Notch restricts the vein fate and affects cell proliferation at
392 the D/V boundary, EGF maintains and induces them (Shimmi et al., 2014). The lack of a
393 notched wing phenotype might also indicate that the repression of Notch signaling by α-PheRS
394 might depend on the presence or absence of a not yet identified co-factor. In any case, we
395 conclude that even in the wing, α-PheRS represses Notch signaling, but different regions of
396 the wing disc respond differently to α-PheRS levels, making the wing disc a more complex
397 system to study the responses to elevated α-PheRS levels.

398 In ovarian follicle cells, the elevated levels of α-PheRS led to an increase in clone size
399 with more cells per clone (Ho *et al.*, 2020). This could theoretically also be explained by an
400 inhibitory effect of α-PheRS on Notch signaling, because Notch is required for the follicle cells
401 to exit the mitotic cycle and switch to the endocycle (Lopez-Schier and St Johnston, 2001) and
402 loss of Notch signaling prevents the epithelial cells from switching from the mitotic cell cycle
403 to the endocycle, leading to over-proliferation of follicle cells (Deng et al., 2001; Shcherbata
404 et al., 2004). Similarly, in adult midguts, elevated α-PheRS interfered with normal homeostasis
405 of ISCs by inducing a typical low Notch signaling phenotype with many more ISCs, EBs, and
406 EEs (Micchelli and Perrimon, 2006; Ohlstein and Spradling, 2007; Zhai et al., 2015). Because
407 α-PheRS levels attenuate Notch signaling in different situations where Notch causes diverse
408 effects, α-PheRS (or a part of it) seems to be a general component of Notch signaling.

409 Repression of Notch signaling through competition with the NICD has been described
410 in different systems and has recently been reviewed (Maier, 2019; Oswald and Kovall, 2018).
411 Best studied is probably the competition involving the factors binding to the C-terminal domain
412 (CTD) of Su(H) (CSL in vertebrates and RBPJ in mammals) that lead to the formation of the
413 Complex of Repressor (CoR) that inhibits Notch target gene activation. A less well-studied
414 group of competitors compete directly with the binding of the RAM domain of the NICD to
415 the BTD of the Su(H) ortholog CSL/RBPJ (Maier, 2019; Oswald and Kovall, 2018). This
416 competition involves the 20 N-terminal amino acids of the RAM domain, which contain the
417 hydrophobic tetrapeptide with the key tryptophane residue (ΦWΦP). So far, this competition
418 was only seen in mammals and, therefore, considered to be specific for vertebrate Notch
419 signaling. These competitors are Epstein-Barr nuclear antigen 2 (EBNA2), mouse
420 KyoT2/FHL1, and human RITA (RBPJ interacting and tubulin associated) (Collins et al., 2014;
421 Johnson et al., 2010; Tabaja et al., 2017; Taniguchi et al., 1998; Wacker et al., 2011; Zimber-
422 Strobl and Strobl, 2001). Our results now show that a naturally occurring fragment of a
423 Drosophila household protein functions through this mechanism to modulate or attenuate
424 Notch signaling and that this is only possible if this invariant W is present. The immediately
425 adjacent hydrophobic residues are also present in the alpha-S tetrapeptide sequence. However,
426 the residue in position four, a proline, is substituted by another hydrophobic residue, leucine.
427 Interestingly, even in mammals, this residue is less conserved than the W in position two
428 (Maier, 2019). Two additional elements have been discussed to affect the affinity of the
429 interaction between the RAM domain and the transcription factor (CSL, RBPJ, or Su(H))
430 (Oswald and Kovall, 2018). The dipeptides -HG– and –GF–. Interestingly, both dipeptides are
431 also present in the N-terminal 20 amino acids of the RAM domain of Drosophila Notch, α-
432 PheRS, and α-S even though they are found in different positions (Fig 7A). Their contribution
433 to the binding affinity would therefore have to be further evaluated. Additionally, the α-S

434 polypeptide also contains a KKRK sequence element that might function as a nuclear
435 localization sequence (NLS). It might therefore allow α-S or α-PheRS$^{(Cys)}$ to enter the nucleus
436 and compete with the NICD for the binding to Su(H). Finally, α-S encodes also the DBD-1,2,
437 and 3 (Fig 6B) with helix-turn-helix (HTH) DNA binding motifs, which might also contribute
438 to the function of the complex with Su(H). Further investigations should determine whether
439 such an interaction between α-S and Su(H) leads to the formation of a transcriptional repressor
440 or even to the degradation of the Su(H) transcription factor. Unfortunately, the functional Su(H)
441 antibody that has been used so far is not available anymore and, in our hands, the new one is
442 too unspecific to draw conclusions.

443 A correlation between elevated levels of α-PheRS or FARSA has been noted some time
444 ago (Sen *et al.*, 1997) and is also suggested by the data published in the GENT2 database (Park
445 *et al.*, 2019). Not the least because colon cancers are among the ones that express higher levels
446 of α-PheRS in the tumor tissue than in the healthy counterpart, modeling the effect of elevated
447 α-PheRS levels in *Drosophila* ISCs and EBs might reveal mechanisms contributing to tumor
448 development. In the gut tissue, elevated α-PheRS and α-PheRS$^{Cys}$ levels produced 12-14 times
449 as many tumors and these showed mostly a more severe phenotype (Fig 3H). Such tumors were
450 composed of ISCs and differentiating EBs. Similarly, guts also contained 5-8 times as many
451 mitotic cells when α-PheRS$^{(Cys)}$ levels were elevated (Fig 3E). Together, these results strongly
452 suggest that higher levels of α-PheRS can induce strong cell proliferation. Additionally,
453 because these over-proliferation cells display stem cell characteristics and changes in cell fate,
454 we suggest that elevated α-PheRS levels should indeed be considered a risk factor for tumor
455 formation.

456 The hyperaccumulation of cells with stem cell characteristics is mediated by high α-
457 PheRS$^{(Cys)}$ or α-S repressing Notch signaling. In mammals, Notch signaling is essential for

458 maintaining the homeostasis of cell proliferation and differentiation (Qiao and Wong, 2009)
459 similar to the function of Notch signaling in the Drosophila gut that is needed to prevent the
460 induction of tumors in the adult midgut (Micchelli and Perrimon, 2006; Ohlstein and Spradling,
461 2007). Because in humans, misregulation of Notch signaling in these processes has been
462 suggested to trigger the development of colon cancer, *Notch* has been proposed as a molecular
463 target for cancer therapy (Yin et al., 2010). The results presented here provide new and
464 unexpected insights into the regulation of Notch signaling in the context of gut tumorigenesis
465 and they suggest new opportunities to target these mechanisms.

466

467 # Materials and Methods

468 ## Key Resources Table

| Reagent or Resource | Sources | Identifier | Additional information |
|---|---|---|---|
| **Antibodies** | | | |
| Anti phospho-Histone H3-rabbit | Cell signaling | 9701S | 1:200 v/v |
| Anti phospho-Histone H3-mouse | Cell signaling | 9706S | 1:200 v/v |
| Anti *α-PheRS* | Genescript | 4668 | Customized product (1:200 v/v) |
| Anti *α-PheRS* | Genescript | 4669 | Customized product (1:200 v/v) |
| Anti Myc-mouse | Developmental Studies Hybridoma Bank (DSHB) | 9E10 | Supernatant (1:3 v/v) |
| Anti Puromycin | DSHB | PMY-2A4 | 1:100 v/v |
| Anti Prospero | DSHB | MR1A | 1:200 v/v |
| Anti Delta | DSHB | C594.9B | 1:10 v/v |
| Anti V5 tag-rabbit | Cell signaling | 13202 | 1:200 v/v |
| Anti Cy3 rabbit | Jackson Immuno Research | 115-165-146 | 1:200 v/v |
| Anti-rabbit Alexa Flour 488 | Molecular Probes | A-11008 | 1:200 v/v |
| Anti-rabbit Alexa Flour 488 | Molecular Probes | A-11034 | 1:200 v/v |
| Anti-mouse Alexa Flour 488 | Molecular Probes | A-11029 | 1:200 v/v |
| Anti-rabbit Alexa Flour 488 | Life technology | A-21206 | 1:200 v/v |
| Anti-rabbit Alexa Flour 594 | Invitrogen | A-11037 | 1:200 v/v |
| Anti-mouse Alexa Flour 594 | Molecular Probes | A-11032 | 1:200 v/v |
| Anti-mouse Alexa Flour 568 | Life technology | A-10037 | 1:200 v/v |
| Anti α-tubulin | Abcam | Ab18251 | 1:1,000 v/v |
| Anti GFP | ImmunoKontact | 042704 | 1:1,000 v/v |
| Anti Myc-rabbit | Santa Cruz | Sc-789 | A-12 (1:1,000 v/v) |
| HRP Anti rabbit IgG antibody (Peroxidase) | Vector | PI-1000 | 1:10,000 v/v |
| HRP Anti rabbit IgG antibody (Peroxidase) | Vector | PI-2000 | 1:10,000 v/v |

469

| **Fly stocks and genetics** | | | |
|---|---|---|---|
| *α-PheRS$^{G2060}$/FM6* | Bloomington Drosophila Stock Center (BDSC) | 26625 | |
| *RNAi- α-PheRS* | Vienna Drosophila RNAi Center (VDRC) | 33514 | |
| *RNAi- β-PheRS* | VDRC | 42046 | |
| *gα-PheRS$^{Cys}$* | | | Transgenic construct |
| *UAS-α-PheRS$^{Cys}$* | | | Transgenic construct |
| *hspFLP ; Act-Gal4/CyO ; neoFRT82B,tub-Gal80/TM3,Sb* | | | |
| *w ; If/CyO ; neoFRT82B,UAS- α-PheRS$^{(Cys)}$* | | | |
| *engrailed-Gal4* | BDSC | 30564 | |
| *engrailed-Gal4,NRE-EGFP,UAS-myrRFP* | BDSC | 30730 | |
| *UAS-GFP* | BDSC | 6658 | |
| *w; UAS-Myc::MYC* | BDSC | 9674 | |
| *hspFLP/y ; + ; UAS-Myc::MYC* | BDSC | 9675 | |
| *hspFLP/y ; UAS-NICD /CyO ; MKRS/TM2* | BDSC | 52008 | |
| *NRE-EGFP* | BDSC | 30727 | |
| *UAS-N RNAi* | BDSC | 7078 | |
| *neoFRT*82B *Sb1*/TM6 | BDSC | 2051 | |
| *NRE-eGFP* | BDSC | 30728 | |
| *UAS-Dl* | BDSC | 5614 | |
| *tub-Gal4/TM3,Sb* | BDSC | 5138 | |
| *w$^{*}$, Insc-Gal4* | BDSC | 8751 | |
| *w$^{*}$,UAS-Dicer2 ; wor-Gal4, ase-Gal80; UAS-mCD8::GFP* | IMBA | | A gift from Juergen A. Knoblich, IMBA |
| *y w att2A[vas-ϕ]; +; attP-86F* | ETH Zurich | | A gift from Hugo Stocker, ETH |
| *esg-Gal4,UAS-2XEYFP;MKRS/TM6B,Tb* | ETH Zurich | | A gift from Hugo Stocker, ETH |
| *esg-Gal4,UAS-2XEYFP;tub-Gal80$^{ts}$/TM3,Sb* | ETH Zurich | | A gift from Hugo Stocker, ETH |
| *yw; esg-Gal4, UAS-GFP/TM6B,Tb,Hu* | ETH Zurich | 2400 | A gift from Hugo Stocker, ETH |
| *NP1-Gal4 (Myo31DF or Myo1A-Gal4)/CyO, y+* | ETH Zurich | 2398 | A gift from Hugo Stocker, ETH |
| *esg-Gal4, UAS-mCherry-CD8, tub-gal80$^{ts}$/CyO* | | | A gift from Péter Nagy, Cornell University |
| *yw;UAS-cyto-gars-myc/CyO* | | | A gift from Albena Jordanova, VIB-U Antwerp Center for Molecular Neurology |

470

471

| **Bacteria strains and vectors** | | |
|---|---|---|
| XL1 blue | Aligent | 200249 |
| Rosseta – Novagen | Merckmilipore | 70954 |
| pET-28a – Novagen | Merckmilipore | 69864 |
| pET LIC (2A-T) | Addgene | 29665 |
| pUASattB | Drosophila Genomics Resource Center | 1419 |
| pw+SNattB | (Koch et al., 2009) | |
| **Commercial assay or kit** | | |
| Pierce® Silver Stain kit | Thermo Scientific | 24612 |
| Pierce® BCA Protein Assay kit | Thermo Scientific | 23227 |
| ReliaPrep™ DNA CleanUp and Concentration System | Promega | A2893 |
| GeneElute™ HP Plasmid miniprep kit | Sigma | NA0160 |
| Qiagen® Plasmid Plus Midi kit | Qiagen | 12943 |
| Ni-NTA affinity resin | Qiagen | 30210 |
| ECL™ Prime Western Blotting System | GE Healthcare | RPN2232 |
| RNAMaxx™ High Yield Transcription Kit | Aligent | 200339 |
| | | |
| **Software, algorithm** | | |
| Leica Application Suite X (LAS X) | Leica | https://www.leica-microsystems.com/products/microscope-software/p/leica-las-x-ls/ |
| FIJI | ImageJ | https://fiji.sc/ |
| GraphPad Prism | GraphPad | https://www.graphpad.com/scientific-software/prism/ |
| FlowJo™ | BD Biosciences | https://www.flowjo.com/ |
| Microsoft Excel | Microsoft | https://products.office.com/en-us/excel |

472

473 **Buffers**

| **Lysis buffer for Drosophila tissue** | **Lysis buffer for bacteria** |
|---|---|
| 20 mM Tris HCl pH7.4<br>150uM NaCl<br>2 mM EDTA<br>50 mM NaF<br>10% Glycerol<br>1% Triton X100<br>1 Protease inhibitor cocktail tablet (Roche-4693159001)<br>1 mM phenylmethylsulphonyl fluoride | 20 mM Tris HCl pH7.4<br>150uM NaCl<br>2 mM EDTA<br>50 mM NaF<br>10% Glycerol<br>1% Triton X100<br>4mM Imidazole 1M<br>0.6% Lysozyme<br>1 Protease inhibitor cocktail tablet<br>1 mM phenylmethylsulphonyl fluoride |
| **4% PFA** | **1X PBST** |
| 1X PBST<br>4% (w/v) Paraformaldehyde | 0.2 % (v/v) Tween 20<br>1X PBS |
| **Blocking buffer** | **Fly food recipe** |

| | |
|---|---|
| 5% (w/v) non-fat dry milk<br>0.1% (v/v) Triton X100 | 20.4 l $H_20$<br>1,680 g Maize flour<br>720 g Yeast<br>1,800 g Syrup<br>192 g Potassium sodium tartrate tetrahydrate<br>36 g Nipagin<br>120 ml Propionic acid |
| **10X PBS pH 7.4** | |
| 10.6 mM $KH_2PO_4$<br>1.5 M NaCl<br>30 mM $Na_2PO_4.7H_20$ | |
| **10X SDS running buffer** | **10X Transfer buffer** |
| 30 g Tris base<br>144 g Glycine<br>10 g SDS<br>$dH_2O$ to 1□ | 30 g Tris base<br>144 g Glycine<br>$dH_2O$ to 1□ |
| **10X TBS pH to 7.6** | **1X TBST** |
| 24 g of Tris Base<br>88 g of NaCl<br>$dH_2O$ to 1□ | 100 mL 10X TBS<br>900 mL $dH_2O$<br>0.1% (v/v) Tween 20 |

474

475 **Primers**

| Name | Sequence (5' to 3') | Application |
|---|---|---|
| rc2263f | CGCGGATCCATCCGGCGAGAGAGTGTCTTTG | Genomic genomic construct of *α-PheRS* |
| rc2263r | CGGGGTACCTATGCCTGGCGATAATCGTG | |
| Tyr412Cys & Phe438Cys-F | TCAAGCCGGCGTACAATCCGTGTACCGAGCCCAG | Construct of *α-PheRS*$^{Cys}$ mutation |
| Tyr412Cys & Phe438Cys-R | CTCCGGCCGACAGACGCCCGAGTTGCCC | |
| *α-PheRS* RNAi 11f | TAATACGACTCACTATAGGGAGGCAAGAAACGCAA GCTCCTC | *α-PheRS* ds RNA synthesis |
| *α-PheRS* RNAi 11r | TAATACGACTCACTATAGGGAGGGAACTCCGCCAG ATGTGTG | |
| *β-PheRS* RNAi 10f | TAATACGACTCACTATAGGGAGGGCCAATCATTCG GGAATCA | *β-PheRS* ds RNA synthesis |
| *β-PheRS* RNAi 10r | TAATACGACTCACTATAGGGAGGAGGCAGGGACTT CTTAATGT | |
| seq r6 | GCTCCCATTCATCAGTTCC | Sequencing |
| seqA r1 | CATTTCCACCGTGAGATCCGTC | Sequencing |
| seqA r2 | AACTCTTGTGGGTGACCGTTTC | Sequencing |
| seqA f1 | GTTCTCGAAGTGAATGTTCTGG | Sequencing |
| seqA f2 | TTTAGCCACCGTCGTCGTTTC | Sequencing |
| seqA r3 | TCCAGCGACGATGACGAATTTG | Sequencing |
| seqA f3 | CAAATGGATTGTGGGACCAGC | Sequencing |
| seqA r4 | GCCCTCCTCCACCATCTTTAG | Sequencing |

476

477 **Fly genetics and husbandry**

478 All *Drosophila melanogaster* fly stocks were kept for long term storage at 18ºC in glass or
479 plastic vials on standard food with day/night (12h/12h) light cycles. All experiments were
480 performed at 25ºC unless specifically mentioned. A UAS-GFP element was added in
481 experiments that tested for rescue and involved Gal4-mediated expression of the rescue gene.
482 This construct served to even out the number of UAS sites in each Gal4 expressing cell. Origins
483 of all stocks are noted in the *Key Resource Table*.

484

485 **DNA cloning and generation of transgenic flies**

486 Sequence information was obtained from Flybase. All mutations and the addition of the Myc-
487 tag to the N-terminus of *α-PheRS* were made by following the procedure of the QuickChange®
488 Site-Directed Mutagenesis Kit (Stratagene). The genomic *α-PheRS* rescue construct (*Myc::α-*
489 *PheRS*) codes for the entire coding region and an additional Myc tag at the N-terminal end. In
490 addition, it contains ~1kb of up- and down-stream sequences and it was cloned into the
491 *pw$^+$SNattB* transformation vector (Koch *et al.*, 2009; Lu *et al.*, 2014). The *α-PheRS* and *β-*
492 *PheRS* cDNAs were obtained by RT-PCR from mRNA isolated from 4-8 days old *OreR* flies
493 (Lu *et al.*, 2014). Transgenic flies were generated by applying the *ϕ* C31-based integration
494 system with the stock (*y w att2A[vas-ϕ]; +; attP-86F*) (Bischof et al., 2007).

495

496 **Western blotting**

497 Protein was extracted from tissues, whole larvae, or flies using lysis buffer. 25 guts were
498 analyzed for each genotype. Protein lysates were separated by SDS-PAGE and transferred onto

499 PVDF membranes (Milipore, US). The blocking was performed for 1h at room temperature
500 (RT) with non-fat dry milk (5%) in TBST solution. Blots were probed first with primary
501 antibodies (diluted in blocking buffer) overnight at 4ºC and then with secondary antibodies
502 (diluted in TBST) 1h at RT. The signal of the secondary antibody was detected by using the
503 detect solution mixture (1:1) (ECL™ Prime Western Blotting System, GE Healthcare Life
504 Science) and a luminescent detector (Amersham Imager 600, GE Healthcare Life Science).
505 Origins and recipes of all buffers and reagents are noted in the *Key Resource Table*.

506

507 **Immunofluorescent staining and confocal microscopy**

508 Adult midguts were dissected from each female fly after 5 days at 29ºC (unless stated
509 otherwise) or at different time points after 2, 3, 4 days of heat treatment for the time-course
510 experiment. A total of 10 guts were analyzed for each genotype. In the larval experiments, the
511 animals were mated at 25ºC on fresh, rich diet food and set up for egg-laying during a 2-hour
512 window. 120 hours after egg-laying, larval midguts were dissected from wandering third instar
513 larvae and a total of 10 guts were analyzed for each genotype. Dissections were performed in
514 1X PBS on ice and tissues were collected within a maximum of one hour. Fixation with 4%
515 PFA in PBS-T 0.2% at RT was done for different durations depending on the different tissues:
516 two hours (guts), 40 minutes (brains), 30 minutes (wing discs, ovaries). Then the samples were
517 blocked overnight with a blocking buffer at 4ºC. Primary antibodies (diluted in blocking buffer)
518 were incubated with the samples for 8h at RT. The samples were rinsed 3 times and washed 3
519 times (20 minutes/wash) with PBST. Secondary antibodies (diluted in PBST) were incubated
520 overnight at 4ºC. The samples were then rinsed 3 times and washed 2 times (20 minutes/wash)
521 with PBST. Hoechst 33258 (2.5 μg/ml) was added in PBST before the third and last washing
522 step and the samples were mounted with Aqua/Poly Mount solution (Polysciences Inc., US).

523 For the anti-Delta labeling, the samples were blocked for 3h at RT with a blocking buffer. The
524 primary anti-Delta antibody (1:10 v/v) was incubated with the samples overnight at 4ºC and
525 then the secondary antibody was incubated overnight at 4ºC. Origins and diluted concentrations
526 of all buffers and antibodies are noted in the *Key Resource Table*.

527

528 **Image acquisition and processing**

529 Imaging was carried out with a Leica SP8 confocal laser scanning microscope equipped with
530 a 405 nm diode laser, a 458, 476, 488, 496, and 514 nm Argon laser, a 561 nm diode pumped
531 solid-state laser, and a 633 nm HeNe laser. Images were obtained with 20x dry and 63x oil-
532 immersion objectives and 1024x1024 pixel format. Images were acquired using LAS X
533 software. The images of the entire gut were obtained by imaging at the standard size and then
534 merging maximal projections of Z-stacks with the Tiles Scan tool. Fluorescent intensity was
535 determined from FIJI software.

536

537 **Quantification of cell numbers per posterior midgut**

538 Z stack images through the width of the posterior midgut were acquired along the length of the
539 posterior midgut from the R4a compartment to the midgut-hindgut junction. Maximum
540 projections of each Z stack were obtained, and the total numbers of each cell type were counted
541 manually and exported to Microsoft Excel and GraphPad Prism for further statistical analysis.

542

543 **Quantification and statistical analysis**

544 For quantifications of all experiments, *n* represents the number of independent biological
545 samples analyzed (the number of guts, the number of wing discs, the number of twin spots),
546 error bars represent standard deviation (SD). Statistical significance was determined using the

547 t-test or ANOVA as noted in the figure legends. They were expressed as P values. (*) denotes
548 $p < 0.05$, (**) denotes $p < 0.01$, (***) denotes $p < 0.001$, (****) denotes $p < 0.0001$. (*ns*)
549 denotes values whose difference was not significant.
550
551
552
553

554 **Acknowledgments**

555 We thank Peter Nagy, Hugo Stocker, Albena Jordanova, Erik Storkebaum, and the
556 Bloomington Stock Center for fly stocks. We are also grateful to Rohan Chippalkatti for
557 sharing his knowledge about the larval brain. This work was supported by the Novartis
558 Foundation for medical-biological Research (#18A050), the Swiss National Fund (project
559 grant 31003A_173188), and the University/Canton of Bern.

# References


Ables, J.L., Breunig, J.J., Eisch, A.J., and Rakic, P. (2011). Not(ch) just development: Notch signalling in the adult brain. Nature reviews. Neuroscience *12*, 269-283. 10.1038/nrn3024.

Barrick, D., and Kopan, R. (2006). The Notch transcription activation complex makes its move. Cell *124*, 883-885. 10.1016/j.cell.2006.02.028.

Beehler-Evans, R., and Micchelli, C.A. (2015). Generation of enteroendocrine cell diversity in midgut stem cell lineages. Development *142*, 654-664. 10.1242/dev.114959.

Biehs, B., Sturtevant, M.A., and Bier, E. (1998). Boundaries in the Drosophila wing imaginal disc organize vein-specific genetic programs. Development *125*, 4245-4257.

Bischof, J., Maeda, R.K., Hediger, M., Karch, F., and Basler, K. (2007). An optimized transgenesis system for Drosophila using germ-line-specific phiC31 integrases. Proceedings of the National Academy of Sciences of the United States of America *104*, 3312-3317. 10.1073/pnas.0611511104.

Borggrefe, T., and Oswald, F. (2009). The Notch signaling pathway: transcriptional regulation at Notch target genes. Cellular and molecular life sciences : CMLS *66*, 1631-1646. 10.1007/s00018-009-8668-7.

Borggrefe, T., and Oswald, F. (2016). Setting the Stage for Notch: The Drosophila Su(H)-Hairless Repressor Complex. PLoS biology *14*, e1002524. 10.1371/journal.pbio.1002524.

Bray, S., and Furriols, M. (2001). Notch pathway: making sense of suppressor of hairless. Current biology : CB *11*, R217-221. 10.1016/s0960-9822(01)00109-9.

Casas-Tinto, S., Lolo, F.N., and Moreno, E. (2015). Active JNK-dependent secretion of Drosophila Tyrosyl-tRNA synthetase by loser cells recruits haemocytes during cell competition. Nature communications *6*, 10022. 10.1038/ncomms10022.

Collins, K.J., Yuan, Z., and Kovall, R.A. (2014). Structure and function of the CSL-KyoT2 corepressor complex: a negative regulator of Notch signaling. Structure *22*, 70-81. 10.1016/j.str.2013.10.010.

de Celis, J.F., de Celis, J., Ligoxygakis, P., Preiss, A., Delidakis, C., and Bray, S. (1996). Functional relationships between Notch, Su(H) and the bHLH genes of the E(spl) complex: the E(spl) genes mediate only a subset of Notch activities during imaginal development. Development *122*, 2719-2728.

de la Pompa, J.L., Wakeham, A., Correia, K.M., Samper, E., Brown, S., Aguilera, R.J., Nakano, T., Honjo, T., Mak, T.W., Rossant, J., and Conlon, R.A. (1997). Conservation of the Notch signalling pathway in mammalian neurogenesis. Development *124*, 1139-1148.

593 Deng, W.M., Althauser, C., and Ruohola-Baker, H. (2001). Notch-Delta signaling induces a
594 transition from mitotic cell cycle to endocycle in Drosophila follicle cells. Development *128*,
595 4737-4746.

596 Finarov, I., Moor, N., Kessler, N., Klipcan, L., and Safro, M.G. (2010). Structure of human
597 cytosolic phenylalanyl-tRNA synthetase: evidence for kingdom-specific design of the active
598 sites and tRNA binding patterns. Structure *18*, 343-353. 10.1016/j.str.2010.01.002.

599 Fortini, M.E., and Artavanis-Tsakonas, S. (1994). The suppressor of hairless protein
600 participates in notch receptor signaling. Cell *79*, 273-282. 10.1016/0092-8674(94)90196-1.

601 Furriols, M., and Bray, S. (2001). A model Notch response element detects Suppressor of
602 Hairless-dependent molecular switch. Current biology : CB *11*, 60-64. 10.1016/s0960-
603 9822(00)00044-0.

604 Giachino, C., and Taylor, V. (2014). Notching up neural stem cell homogeneity in
605 homeostasis and disease. Frontiers in neuroscience *8*, 32. 10.3389/fnins.2014.00032.

606 Gomard-Mennesson, E., Fabien, N., Cordier, J.F., Ninet, J., Tebib, J., and Rousset, H. (2007).
607 Clinical significance of anti-histidyl-tRNA synthetase (Jo1) autoantibodies. Annals of the
608 New York Academy of Sciences *1109*, 414-420. 10.1196/annals.1398.047.

609 Gordon, W.R., Arnett, K.L., and Blacklow, S.C. (2008). The molecular logic of Notch
610 signaling--a structural and biochemical perspective. Journal of cell science *121*, 3109-3119.
611 10.1242/jcs.035683.

612 Grandbarbe, L., Bouissac, J., Rand, M., Hrabe de Angelis, M., Artavanis-Tsakonas, S., and
613 Mohier, E. (2003). Delta-Notch signaling controls the generation of neurons/glia from neural
614 stem cells in a stepwise process. Development *130*, 1391-1402.

615 Greenberg, Y., King, M., Kiosses, W.B., Ewalt, K., Yang, X., Schimmel, P., Reader, J.S., and
616 Tzima, E. (2008). The novel fragment of tyrosyl tRNA synthetase, mini-TyrRS, is secreted to
617 induce an angiogenic response in endothelial cells. FASEB journal : official publication of
618 the Federation of American Societies for Experimental Biology *22*, 1597-1605.
619 10.1096/fj.07-9973com.

620 Guo, M., and Schimmel, P. (2013). Essential nontranslational functions of tRNA synthetases.
621 Nature chemical biology *9*, 145-153. 10.1038/nchembio.1158.

622 Guo, Z., Lucchetta, E., Rafel, N., and Ohlstein, B. (2016). Maintenance of the adult
623 Drosophila intestine: all roads lead to homeostasis. Current opinion in genetics &
624 development *40*, 81-86. 10.1016/j.gde.2016.06.009.

625 Guo, Z., and Ohlstein, B. (2015). Stem cell regulation. Bidirectional Notch signaling
626 regulates Drosophila intestinal stem cell multipotency. Science *350*.
627 10.1126/science.aab0988.

628 Hatakeyama, J., Bessho, Y., Katoh, K., Ookawara, S., Fujioka, M., Guillemot, F., and
629 Kageyama, R. (2004). Hes genes regulate size, shape and histogenesis of the nervous system
630 by control of the timing of neural stem cell differentiation. Development *131*, 5539-5550.
631 10.1242/dev.01436.

632 Henrique, D., and Schweisguth, F. (2019). Mechanisms of Notch signaling: a simple logic
633 deployed in time and space. Development *146*. 10.1242/dev.172148.

634 Ho, M.T., Lu, J., and Suter, B. (2020). An aminoacylation independent activity of
635 PheRS/FARS promotes growth and proliferation. bioRxiv, 2020.2010.2029.360420.
636 10.1101/2020.10.29.360420.

637 Hori, K., Sen, A., and Artavanis-Tsakonas, S. (2013). Notch signaling at a glance. Journal of
638 cell science *126*, 2135-2140. 10.1242/jcs.127308.

639 Houtz, P., Bonfini, A., Bing, X., and Buchon, N. (2019). Recruitment of Adult Precursor
640 Cells Underlies Limited Repair of the Infected Larval Midgut in Drosophila. Cell host &
641 microbe *26*, 412-425 e415. 10.1016/j.chom.2019.08.006.

642 Jiang, H., and Edgar, B.A. (2011). Intestinal stem cells in the adult Drosophila midgut.
643 Experimental cell research *317*, 2780-2788. 10.1016/j.yexcr.2011.07.020.

644 Johannes, B., and Preiss, A. (2002). Wing vein formation in Drosophila melanogaster:
645 hairless is involved in the cross-talk between Notch and EGF signaling pathways.
646 Mechanisms of development *115*, 3-14. 10.1016/s0925-4773(02)00083-7.

647 Johnson, S.E., Ilagan, M.X., Kopan, R., and Barrick, D. (2010). Thermodynamic analysis of
648 the CSL x Notch interaction: distribution of binding energy of the Notch RAM region to the
649 CSL beta-trefoil domain and the mode of competition with the viral transactivator EBNA2. J
650 Biol Chem *285*, 6681-6692. 10.1074/jbc.M109.019968.

651 Koch, R., Ledermann, R., Urwyler, O., Heller, M., and Suter, B. (2009). Systematic
652 functional analysis of Bicaudal-D serine phosphorylation and intragenic suppression of a
653 female sterile allele of BicD. PloS one *4*, e4552. 10.1371/journal.pone.0004552.

654 Kovall, R.A. (2007). Structures of CSL, Notch and Mastermind proteins: piecing together an
655 active transcription complex. Current opinion in structural biology *17*, 117-127.
656 10.1016/j.sbi.2006.11.004.

657 Lee, J.H., and Lee, W.J. (2019). Stealing from the Future: Injured Larvae Spend Stem Cell
658 Deposits. Cell host & microbe *26*, 301-303. 10.1016/j.chom.2019.08.013.

659 Lee, S.W., Cho, B.H., Park, S.G., and Kim, S. (2004). Aminoacyl-tRNA synthetase
660 complexes: beyond translation. Journal of cell science *117*, 3725-3734. 10.1242/jcs.01342.

661 Lian, T., Wu, Q., Hodge, B.A., Wilson, K.A., Yu, G., and Yang, M. (2018). Drosophila Gut-
662 A Nexus Between Dietary Restriction and Lifespan. International journal of molecular
663 sciences *19*. 10.3390/ijms19123810.

664 Ling, J., Yadavalli, S.S., and Ibba, M. (2007). Phenylalanyl-tRNA synthetase editing defects
665 result in efficient mistranslation of phenylalanine codons as tyrosine. RNA *13*, 1881-1886.
666 10.1261/rna.684107.

667 Liu, J., Sato, C., Cerletti, M., and Wagers, A. (2010). Notch signaling in the regulation of
668 stem cell self-renewal and differentiation. Current topics in developmental biology *92*, 367-
669 409. 10.1016/S0070-2153(10)92012-7.

670 Lopez-Schier, H., and St Johnston, D. (2001). Delta signaling from the germ line controls the
671 proliferation and differentiation of the somatic follicle cells during Drosophila oogenesis.
672 Genes & development *15*, 1393-1405. 10.1101/gad.200901.

673 Loza-Coll, M.A., Southall, T.D., Sandall, S.L., Brand, A.H., and Jones, D.L. (2014).
674 Regulation of Drosophila intestinal stem cell maintenance and differentiation by the
675 transcription factor Escargot. The EMBO journal *33*, 2983-2996. 10.15252/embj.201489050.

676 Lu, J., Bergert, M., Walther, A., and Suter, B. (2014). Double-sieving-defective aminoacyl-
677 tRNA synthetase causes protein mistranslation and affects cellular physiology and
678 development. Nature communications *5*, 5650. 10.1038/ncomms6650.

679 Maier, D. (2019). The evolution of transcriptional repressors in the Notch signaling pathway:
680 a computational analysis. Hereditas *156*, 5. 10.1186/s41065-019-0081-0.

681 Marianes, A., and Spradling, A.C. (2013). Physiological and stem cell compartmentalization
682 within the Drosophila midgut. eLife *2*, e00886. 10.7554/eLife.00886.

683 Mathur, D., Bost, A., Driver, I., and Ohlstein, B. (2010). A transient niche regulates the
684 specification of Drosophila intestinal stem cells. Science *327*, 210-213.
685 10.1126/science.1181958.

686 Micchelli, C.A. (2012). The origin of intestinal stem cells in Drosophila. Developmental
687 dynamics : an official publication of the American Association of Anatomists *241*, 85-91.
688 10.1002/dvdy.22759.

689 Micchelli, C.A., and Perrimon, N. (2006). Evidence that stem cells reside in the adult
690 Drosophila midgut epithelium. Nature *439*, 475-479. 10.1038/nature04371.

691 Mundorf, J., Donohoe, C.D., McClure, C.D., Southall, T.D., and Uhlirova, M. (2019). Ets21c
692 Governs Tissue Renewal, Stress Tolerance, and Aging in the Drosophila Intestine. Cell
693 reports *27*, 3019-3033 e3015. 10.1016/j.celrep.2019.05.025.

694 Nagel, A.C., Auer, J.S., Schulz, A., Pfannstiel, J., Yuan, Z., Collins, C.E., Kovall, R.A., and
695 Preiss, A. (2017). Phosphorylation of Suppressor of Hairless impedes its DNA-binding
696 activity. Scientific reports *7*, 11820. 10.1038/s41598-017-11952-0.

697 Nagy, P., Sandor, G.O., and Juhasz, G. (2018). Autophagy maintains stem cells and intestinal
698 homeostasis in Drosophila. Scientific reports *8*, 4644. 10.1038/s41598-018-23065-3.

699 Nathanson, L., and Deutscher, M.P. (2000). Active aminoacyl-tRNA synthetases are present
700 in nuclei as a high molecular weight multienzyme complex. The Journal of biological
701 chemistry *275*, 31559-31562. 10.1074/jbc.C000385200.

702 Ohlstein, B., and Spradling, A. (2006). The adult Drosophila posterior midgut is maintained
703 by pluripotent stem cells. Nature *439*, 470-474. 10.1038/nature04333.

704 Ohlstein, B., and Spradling, A. (2007). Multipotent Drosophila intestinal stem cells specify
705 daughter cell fates by differential notch signaling. Science *315*, 988-992.
706 10.1126/science.1136606.

707 Oswald, F., and Kovall, R.A. (2018). CSL-Associated Corepressor and Coactivator
708 Complexes. Adv Exp Med Biol *1066*, 279-295. 10.1007/978-3-319-89512-3_14.

709 Otani, A., Slike, B.M., Dorrell, M.I., Hood, J., Kinder, K., Ewalt, K.L., Cheresh, D.,
710 Schimmel, P., and Friedlander, M. (2002). A fragment of human TrpRS as a potent
711 antagonist of ocular angiogenesis. Proceedings of the National Academy of Sciences of the
712 United States of America *99*, 178-183. 10.1073/pnas.012601899.

713 Park, S.J., Yoon, B.H., Kim, S.K., and Kim, S.Y. (2019). GENT2: an updated gene
714 expression database for normal and tumor tissues. BMC medical genomics *12*, 101.
715 10.1186/s12920-019-0514-7.

716 Praxenthaler, H., Nagel, A.C., Schulz, A., Zimmermann, M., Meier, M., Schmid, H., Preiss,
717 A., and Maier, D. (2017). Hairless-binding deficient Suppressor of Hairless alleles reveal
718 Su(H) protein levels are dependent on complex formation with Hairless. PLoS genetics *13*,
719 e1006774. 10.1371/journal.pgen.1006774.

720 Qiao, L., and Wong, B.C. (2009). Role of Notch signaling in colorectal cancer.
721 Carcinogenesis *30*, 1979-1986. 10.1093/carcin/bgp236.

722 Rodova, M., Ankilova, V., and Safro, M.G. (1999). Human phenylalanyl-tRNA synthetase:
723 cloning, characterization of the deduced amino acid sequences in terms of the structural
724 domains and coordinately regulated expression of the alpha and beta subunits in chronic
725 myeloid leukemia cells. Biochemical and biophysical research communications *255*, 765-
726 773. 10.1006/bbrc.1999.0141.

727 Roy, H., and Ibba, M. (2006). Phenylalanyl-tRNA synthetase contains a dispensable RNA-
728 binding domain that contributes to the editing of noncognate aminoacyl-tRNA. Biochemistry
729 *45*, 9156-9162. 10.1021/bi060549w.

730 Saj, A., Arziman, Z., Stempfle, D., van Belle, W., Sauder, U., Horn, T., Durrenberger, M.,
731 Paro, R., Boutros, M., and Merdes, G. (2010). A combined ex vivo and in vivo RNAi screen
732 for notch regulators in Drosophila reveals an extensive notch interaction network.
733 Developmental cell *18*, 862-876. 10.1016/j.devcel.2010.03.013.

734 Schimmel, P.R., and Soll, D. (1979). Aminoacyl-tRNA synthetases: general features and
735 recognition of transfer RNAs. Annual review of biochemistry *48*, 601-648.
736 10.1146/annurev.bi.48.070179.003125.

737 Sen, S., Zhou, H., Ripmaster, T., Hittelman, W.N., Schimmel, P., and White, R.A. (1997).
738 Expression of a gene encoding a tRNA synthetase-like protein is enhanced in tumorigenic
739 human myeloid leukemia cells and is cell cycle stage- and differentiation-dependent.
740 Proceedings of the National Academy of Sciences of the United States of America *94*, 6164-
741 6169.

742 Shcherbata, H.R., Althauser, C., Findley, S.D., and Ruohola-Baker, H. (2004). The mitotic-
743 to-endocycle switch in Drosophila follicle cells is executed by Notch-dependent regulation of
744 G1/S, G2/M and M/G1 cell-cycle transitions. Development *131*, 3169-3181.
745 10.1242/dev.01172.

746 Shimmi, O., Matsuda, S., and Hatakeyama, M. (2014). Insights into the molecular
747 mechanisms underlying diversified wing venation among insects. Proceedings. Biological
748 sciences *281*, 20140264. 10.1098/rspb.2014.0264.

749 Smirnova, E.V., Lakunina, V.A., Tarassov, I., Krasheninnikov, I.A., and Kamenski, P.A.
750 (2012). Noncanonical functions of aminoacyl-tRNA synthetases. Biochemistry. Biokhimiia
751 *77*, 15-25. 10.1134/S0006297912010026.

752 Tabaja, N., Yuan, Z., Oswald, F., and Kovall, R.A. (2017). Structure-function analysis of
753 RBP-J-interacting and tubulin-associated (RITA) reveals regions critical for repression of
754 Notch target genes. J Biol Chem *292*, 10549-10563. 10.1074/jbc.M117.791707.

755 Taniguchi, Y., Furukawa, T., Tun, T., Han, H., and Honjo, T. (1998). LIM protein KyoT2
756 negatively regulates transcription by association with the RBP-J DNA-binding protein. Mol
757 Cell Biol *18*, 644-654. 10.1128/MCB.18.1.644.

758 Teleman, A.A., and Cohen, S.M. (2000). Dpp gradient formation in the Drosophila wing
759 imaginal disc. Cell *103*, 971-980. 10.1016/s0092-8674(00)00199-9.

760 Thurmond, J., Goodman, J.L., Strelets, V.B., Attrill, H., Gramates, L.S., Marygold, S.J.,
761 Matthews, B.B., Millburn, G., Antonazzo, G., Trovisco, V., et al. (2019). FlyBase 2.0: the
762 next generation. Nucleic acids research *47*, D759-D765. 10.1093/nar/gky1003.

763 Wacker, S.A., Alvarado, C., von Wichert, G., Knippschild, U., Wiedenmann, J., Clauss, K.,
764 Nienhaus, G.U., Hameister, H., Baumann, B., Borggrefe, T., et al. (2011). RITA, a novel
765 modulator of Notch signalling, acts via nuclear export of RBP-J. EMBO J *30*, 43-56.
766 10.1038/emboj.2010.289.

767 Yin, L., Velazquez, O.C., and Liu, Z.J. (2010). Notch signaling: emerging molecular targets
768 for cancer therapy. Biochemical pharmacology *80*, 690-701. 10.1016/j.bcp.2010.03.026.

769 Zeng, X., and Hou, S.X. (2015). Enteroendocrine cells are generated from stem cells through
770 a distinct progenitor in the adult Drosophila posterior midgut. Development *142*, 644-653.
771 10.1242/dev.113357.

772 Zhai, Z., Boquete, J.P., and Lemaitre, B. (2017). A genetic framework controlling the
773 differentiation of intestinal stem cells during regeneration in Drosophila. PLoS genetics *13*,
774 e1006854. 10.1371/journal.pgen.1006854.

775 Zhai, Z., Kondo, S., Ha, N., Boquete, J.P., Brunner, M., Ueda, R., and Lemaitre, B. (2015).
776 Accumulation of differentiating intestinal stem cell progenies drives tumorigenesis. Nature
777 communications *6*, 10219. 10.1038/ncomms10219.

778 Zhou, J.J., Wang, F., Xu, Z., Lo, W.S., Lau, C.F., Chiang, K.P., Nangle, L.A., Ashlock,
779 M.A., Mendlein, J.D., Yang, X.L., et al. (2014). Secreted histidyl-tRNA synthetase splice
780 variants elaborate major epitopes for autoantibodies in inflammatory myositis. The Journal of
781 biological chemistry *289*, 19269-19275. 10.1074/jbc.C114.571026.

782 Zimber-Strobl, U., and Strobl, L.J. (2001). EBNA2 and Notch signalling in Epstein-Barr
783 virus mediated immortalization of B lymphocytes. Semin Cancer Biol *11*, 423-434.
784 10.1006/scbi.2001.0409.

785

786

787 **Figure legends:**

788

789 **Figure 1: α-PheRS is enriched in *Drosophila* intestinal stem cells and elevated α-PheRS**
790 **levels change midgut development.**

791 (A-A", B, C-C", D) α-PheRS accumulation is higher in small, diploid progenitor cells in wild-
792 type adult and larval midguts. Signal intensity values in the graphs (right column) were
793 measured from left to right along the lines in B and D. (E) *α-PheRS* or *α-PheRS*$^{Cys}$ expression
794 was increased by using the *esg-Gal4,UAS-2XEYFP;tub-Gal80*$^{ts}$ (=*esg*$^{ts}$) system that allowed
795 us to control the expression time to study the kinetics of the appearance of the phenotypes. The
796 kinetics of the *Notch* knockdown was similar to the one of *PheRS*$^{(Cys)}$ expression *(esg*$^{ts}$ / *UAS-*
797 *α-PheRS*$^{(Cys)}$*)*. Animals were mated at 18ºC and adults of the required genotypes were collected
798 and shifted to 29ºC to inactivate Gal80$^{ts}$. Adult midguts were dissected from female flies after
799 the indicated induction times.

800

801

802 **Figure 2: Elevated α-PheRS levels affect gut homeostasis, leading to additional progenitor**
803 **cells, EEs, and differentiating EBs.**

804 (A-C"') Elevated α-PheRS or α-PheRS$^{Cys}$ levels induced by the *esg*$^{ts}$ system (see Fig 1E for
805 details) led to additional YFP-positive cells and also to the accumulation of EEs *(esg*$^{ts}$*/+;UAS-*
806 *α-PheRS*$^{(Cys)}$*/+)*. (D-D"') Knockdown of *Notch (N)* with the same *esg*$^{ts}$ system led to a similar
807 phenotype as elevation of α-PheRS levels *(UAS-N*$^{RNAi}$*/+; esg*$^{ts}$*/+)*. (E-F"') Elevation of α-
808 PheRS levels rescued the depleted ISC pool caused by Notch over-activation (induced by
809 expressing the NICD under *esg*$^{ts}$ control). (G) Quantification of YFP$^{+}$ cell numbers. (H)
810 Proportional contribution of EEs to the total number of gut cells in the intestinal region
811 analyzed. (I) Percentage of differentiating EBs among YFP$^{+}$ cells. In all experiments, EEs were
812 visualized with the anti-Prospero antibody, YFP$^{-}$/Hoechst$^{+}$ polyploid cells were counted as
813 ECs. Animals were mated at 18ºC and adults of the required genotypes were collected and
814 shifted to 29ºC to inactivate Gal80$^{ts}$. Adult midguts were dissected from female flies after 5
815 days of induction at 29ºC. At least 10 guts were analyzed for each genotype. n=10, **p<0.01,
816 ***p<0.001, ****p<0.0001 in ANOVA tests.

817

818

819 **Figure 3: Elevated α-PheRS levels lead to a *Notch*-like phenotype in larval guts.**

820 (A-D) Whole gut images and (A'-D') high power micrographs of the posterior midgut area
821 marked with a white square in the overview picture. The expression of the different genes
822 indicated was driven with the *esg-Gal4,UAS-2XEYFP* system. The YFP signal displayed in
823 green marks AMPs and EBs, Hoechst (blue) marks the nuclear DNA. (C) Elevated *α-PheRS*$^{Cys}$
824 expression gave rise to tumor-like areas in both the anterior and the posterior midgut (outlined
825 with dashed lines) (*esg-Gal4,UAS-2XEYFP/+;UAS-α-PheRS*$^{(Cys)}$*/+)*. (E-E", F) Mitotic cells
826 were identified with anti-phospho-Histone H3 (PH3) antibodies (red channel). n=10,

827 **p<0.01, ***p<0.001 in t-tests. (G) Total cells per intestinal region were measured by
828 counting Hoechst 33258 labeled cells manually. n=10, **p<0.01,****p<0.0001. (H) The
829 Notch activity reporter (NRE-eGFP) expresses GFP under the control of a Notch response
830 element. Its levels drastically decreased upon elevated expression of *α-PheRS* or *α-PheRS*$^{Cys}$
831 in adult midgut ISCs (*esg-Gal4,UAS-2XEYFP/+;tub-Gal80*$^{ts}$*/UAS-α-PheRS*$^{(Cys)}$*,NRE-eGFP)*.
832 Female flies were collected 3 days after eclosure and cultured at 29°C for 5 days before
833 dissecting and harvesting their midguts.

834

835

836 **Figure 4: *α-PheRS* counteracts *Notch* activity in neuroblast proliferation.**

837 (A-A") Additional expression of *α-PheRS* or *α-PheRS*$^{Cys}$ in neuroblasts reduced the ratio of
838 central brain (CB) size to optic lobe (OL) size. The *insc-Gal4,UAS-GFP* system was used to
839 drive the expression of the test genes in neuroblasts (NBs) (*w*$^{*}$*, Insc-Gal4/UAS-GFP;UAS-α-*
840 *PheRS*$^{(Cys)}$*/+)*. NBs were labeled by GFP expression. CBs are shown on the right side (area
841 with GFP$^{+}$ NBs and outlined by white dashed lines) and the OL area on the left. (B) Effect of
842 increased expression of *α-PheRS*$^{(Cys)}$and *NICD,* and of *N* knockdown on the CB/OL size ratio.
843 n=20, ***p<0.001, *ns*: not significant. (C-H, I) Elevated α-PheRS or α-PheRS$^{Cys}$ levels
844 reduced the number of Type II NBs per brain lobe, and less than half of the lobes contained the
845 normal 7-8 NBs. *Notch* RNAi caused the same phenotype with higher expressivity. Additional
846 expression of *α-PheRS*$^{(Cys)}$ rescued the tumor phenotype caused by ectopic Notch activation in
847 NB to normal wild-type levels. The larval brains were dissected from third instar larvae, and
848 at least 20 brains were analyzed for each genotype (*w*$^{*}$*,UAS-Dicer2/+;wor-Gal4,ase-*
849 *Gal80/+;UAS-mCD8::GFP/UAS-α-PheRS*$^{(Cys)}$*).* Each brain lobe was classified according to
850 the number of Type II NBs per brain lobe. n = 25.

851

852

853 **Figure 5: Elevated α-PheRS levels repress Notch signaling in wing discs and induce a**
854 ***Notch* phenotype in adult wings.**

855 (A-A"') The ectopic wing venation phenotype resulting from elevated levels of α-PheRS$^{(Cys)}$
856 is similar to the phenotype of *N*$^{RNAi}$ treatment. An ectopic vein branches from the connecting
857 vein between the L4 and L5 vein (arrowhead). Knockdown of *Notch* shows this phenotype and
858 the classical notched phenotype in the distal region of L3, L4, and near the L5 vein. The *en-*
859 *Gal4,tub-Gal80*$^{ts}$ (hereby *en*$^{ts}$) system was used to drive transgene expression in the posterior
860 compartment of developing wing discs *(en*$^{ts}$*/UAS-α-PheRS*$^{(Cys)}$*).* Animals were initially kept at
861 18°C for 3 days and then shifted to 29°C to inactivate Gal80$^{ts}$ until adult flies hatched, enabling
862 expression of α-PheRS, α-PheRS$^{Cys}$ or *N*$^{RNAi}$. (B) Schematic illustration of wild-type wing
863 imaginal discs showing the position of the different compartments; (B') the expression domain
864 of *en*$^{ts}$>mRFP and (B") the expression domain of *NRE-eGFP* along the dorsal/ventral (D/V)
865 boundary. (B"') *en-Gal4,NRE-eGFP,UAS-mRFP;tub-Gal80*$^{ts}$ was used to drive transgene
866 expression in the posterior compartment of developing wing discs and to evaluate the Notch
867 activity with the reporter *NRE-eGFP* (black arrowhead) *(w,UAS-Dcr2/+;en-Gal4,UAS-*
868 *mRFP,NRE-eGFP/+;tub-Gal80*$^{ts}$*/UAS-α-PheRS*$^{(Cys)}$*).* (C-F"') Elevated α-PheRS or α-

PheRS$^{Cys}$ leads to the loss of NRE-eGFP expression in the posterior compartment, similar to the phenotype of *Notch* knockdown *(w,UAS-Dcr2/UAS-N$^{RNAi}$;en-Gal4,UAS-mRFP,NRE-eGFP/+;tub-Gal80$^{ts}$/+)*. After egg-laying and being kept at 18ºC for 6 days, the animals were shifted to 29ºC for 1 day to inactivate Gal80$^{ts}$ and to enable expression of α-PheRS, α-PheRS$^{Cys}$, or *N*$^{RNAi}$.

**Figure 6: The N-terminal 200 amino acids of α-PheRS (α-S) are sufficient to repress Notch activity.**

(A) 3D model of the α-PheRS structure (suggested by SWISS MODEL tool https://swissmodel.expasy.org/) also shows that the catalytic module and the winged DBDs are separated from each other by a linker strand. (B) Schematic illustration of the α-PheRS polypeptide with its ATP and phenylalanine binding residues. α-PheRS has the catalytic domains located in the C-terminal part, and the DNA binding domains (DBD-1,2,3) located in the N-terminal region. The Myc tagged α-S construct lacks all core domains of α-PheRS but encodes the first 200 codons of the α-PheRS ORF under UAS control. (C,D) *Myc::α-S* was expressed using the *esg$^{ts}$* system in adult and larval midguts and this led to similar phenotypes as elevated expression of α-PheRS$^{(Cys)}$ in the same system *(esg$^{ts}$/UAS-Myc::α-S)*. (E-E',F,G) Quantification of PH3$^{+}$ cell numbers (F) and the ratio of EE/EC (G) in the intestinal region analyzed. In all experiments, EEs were visualized with the anti-Prospero antibody, YFP$^{-}$/Hoechst$^{+}$ polyploid cells were counted as ECs. Animals were mated at 18ºC and adults of the required genotypes were collected and shifted to 29ºC to inactivate Gal80$^{ts}$. Adult midguts were dissected from female flies after a 5 days induction at 29ºC. At least 10 guts were analyzed for each genotype. n=10, **p<0.01, ***p<0.001, ****p<0.0001 in ANOVA tests. (H, H') The ectopic wing venation phenotype resulting from elevated levels of Myc::α-S was similar to the phenotype of elevated α-PheRS$^{(Cys)}$ (shown in Fig 5A). An ectopic vein branches from the connecting vein between the L4 and L5 veins (arrowhead). The same system and experimental settings were used as in Fig 5A *(en$^{ts}$/+;UAS-Myc::α-S/+)*. (I-J') Elevated Myc::α-S leads to the loss of NRE-eGFP expression in the posterior compartments, similar to the effect of α-PheRS$^{(Cys)}$. The same system and experimental setup were used as in Fig 5B-F *(w,UAS-Dcr2/+;en-Gal4,UAS-mRFP,NRE-eGFP/+;tub-Gal80$^{ts}$/UAS-Myc::α-S)*. (K, L) Besides the full-length α-PheRS isoform (55kDa), one stable Myc-tag containing isoform around 40 KDa and another around 25KDa appear when expressing transgenic Myc::α-PheRS under the control of the *Tub-Gal4* driver *(w; +/+ ; Tub-Gal4/UAS-Myc::α-PheRS)*. The 40 KDa isoform was present in larval heads and fat bodies, while the 25 KDa isoform was predominantly expressed in larval guts.

908 **Figure 7: Similarity between the Notch RAM domain and α-S suggests competition for a**
909 **common target.**

910 The alignment of Notch and α-PheRS shows that moderately conserved motives are present in
911 the RAM domain and the N-terminal sequence of α-PheRS (A). (C-C"',D-D"') Elevated
912 *Myc::α-S$^{W112A}$* or *α-PheRS$^{W112A}$* levels induced by the *esg$^{ts}$* system (see Fig 1E for details) could
913 not lead to additional YFP-positive cells and also not to the accumulation of EEs *(esg$^{ts}$/+;UAS-*
914 *α-PheRS/+)*. (E-E"',F-F"') Neither elevated Myc::α-S$^{W112A}$ nor α-PheRS$^{W112A}$ levels rescued
915 the depleted ISC pool caused by Notch over-activation (induced by expressing the NICD under
916 the same control). Note that F shows only 2 Pros$^{+}$ cells, the weaker signals are caused by
917 autofluorescence from some fibers (G) Quantification of YFP$^{+}$ cell numbers. (H) Proportional
918 contribution of EEs to the total number of gut cells in the intestinal region analyzed. Animals
919 were mated at 18$^{o}$C and adults of the required genotypes were collected and shifted to 29$^{o}$C to
920 inactivate Gal80$^{ts}$. Adult midguts were dissected from female flies after 5 days of induction at
921 29$^{o}$C. At least 10 guts were analyzed for each genotype. n=10, **p<0.01, ***p<0.001,
922 ****p<0.0001 in ANOVA tests.

923

924

925

926

927

928 **Supplementary figure legends**

929

930 **Figure S1:** The Myc-tagged isoforms from whole larvae were purified by immunoprecipitation
931 and gel purification. The tryptic peptide fragments of the 25kDa band were subsequently
932 analyzed by mass spectrometry (MS). The MS data analysis revealed the peptide coverage of
933 the 25KDa isoform according to the score of Peptide Spectrum Matches (PSM). The 25 KDa
934 isoform contains the peptides of the N-terminal 28% of the full-length α-PheRS.

**Figure 1**

Adult midgut

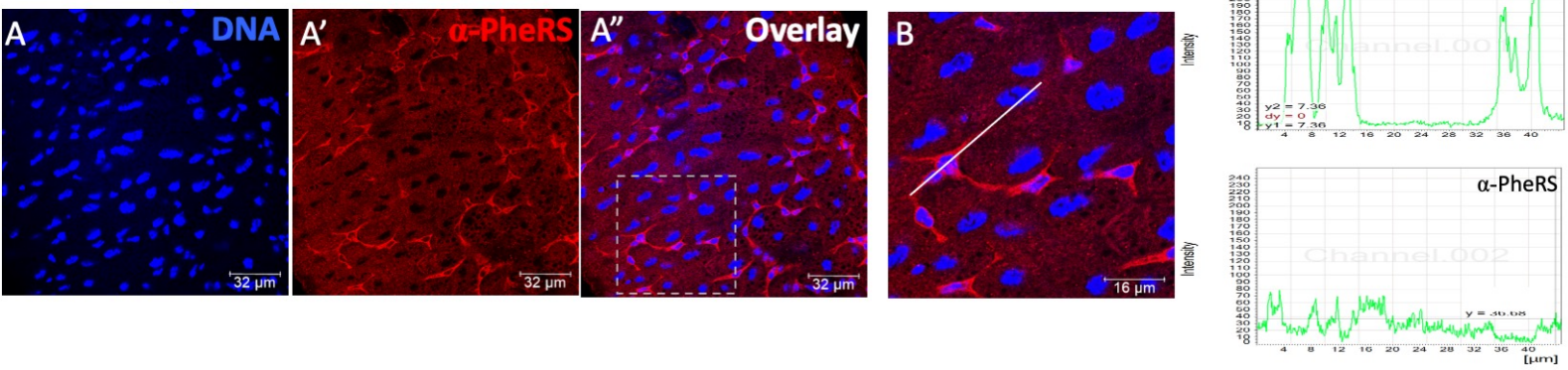


Larval midgut

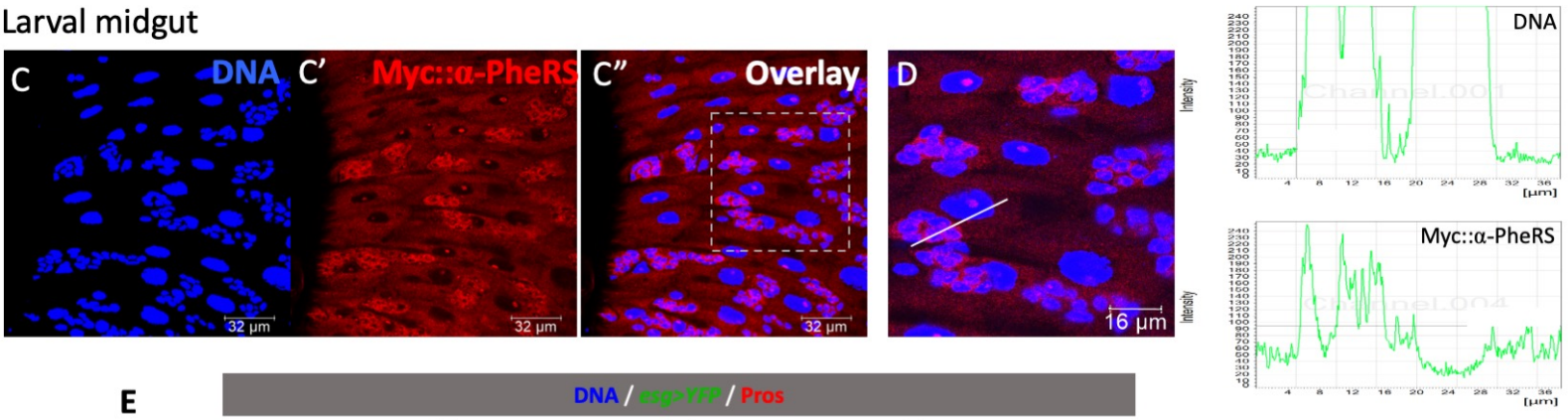


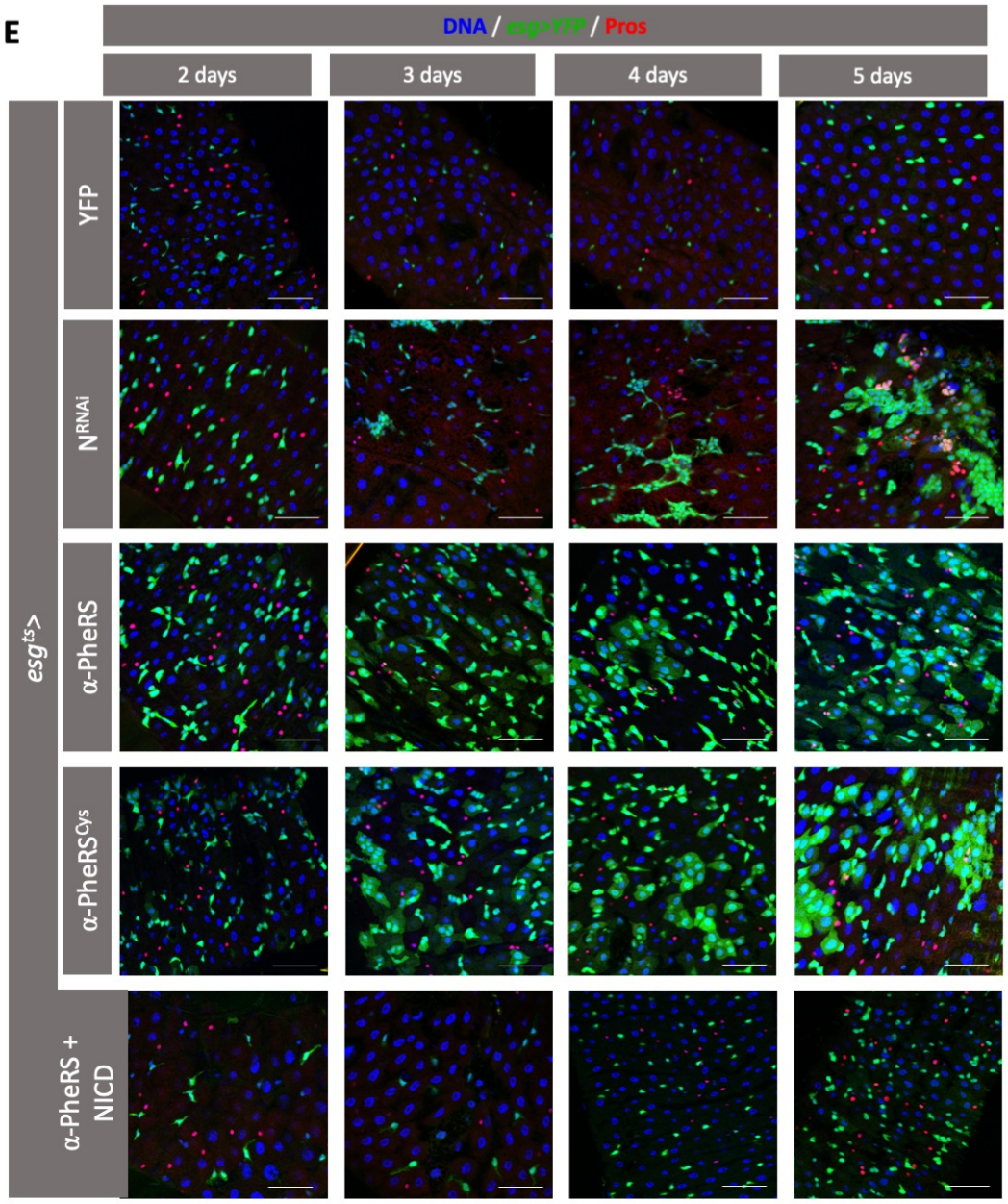

**Figure 2**

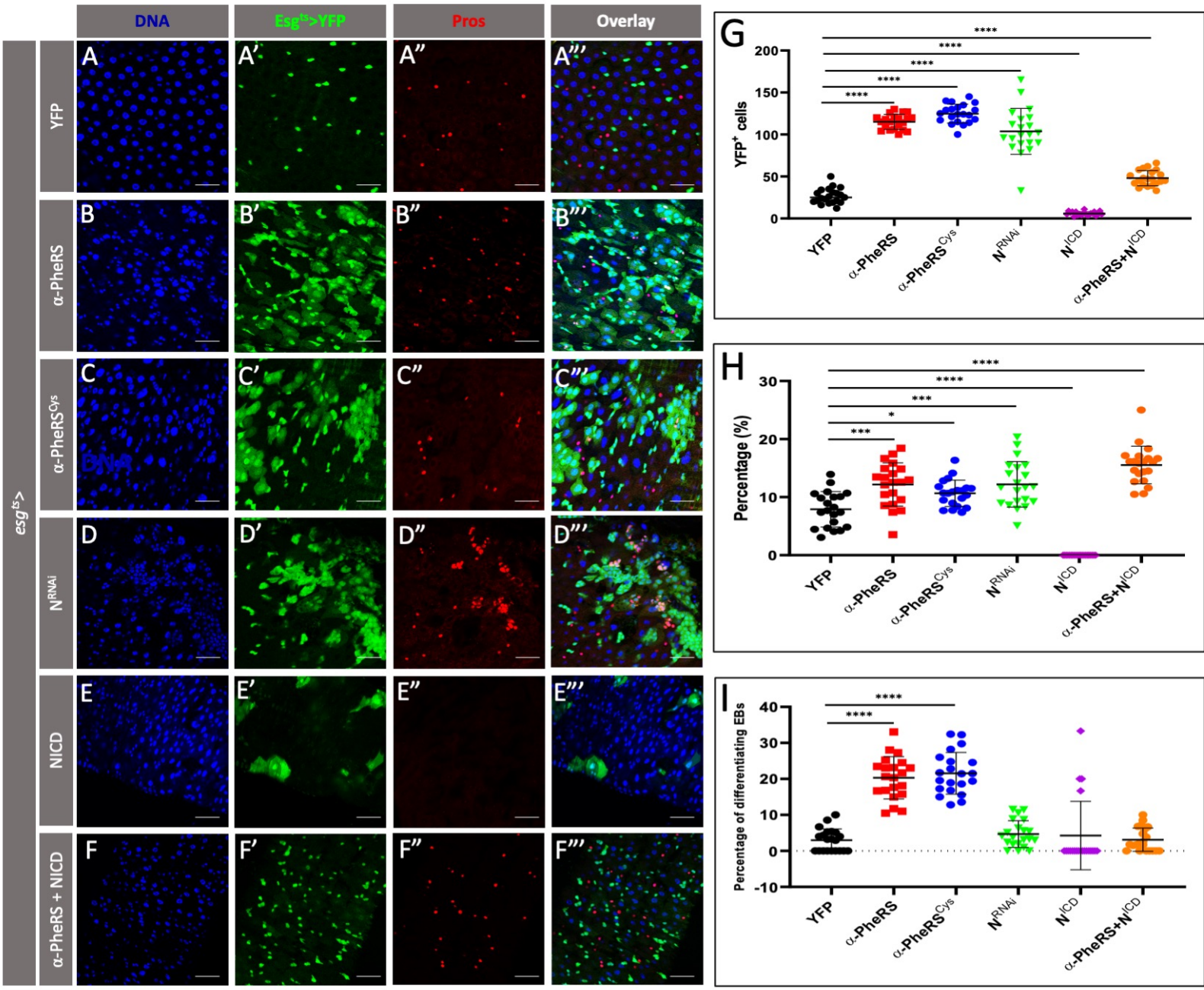
DNA
Esg^ts>YFP
Pros
Overlay
esg^ts>
YFP
α-PheRS
α-PheRS^Cys
N^RNAi
NICD
α-PheRS + NICD
A
A'
A''
A'''
B
B'
B''
B'''
C
C'
C''
C'''
D
D'
D''
D'''
E
E'
E''
E'''
F
F'
F''
F'''
G
YFP+ cells
200
150
100
50
0
****
YFP
α-PheRS
α-PheRS^Cys
N^RNAi
N^ICD
α-PheRS+N^ICD
H
Percentage (%)
30
20
10
0
***
*
I
Percentage of differentiating EBs
40
30
20
10
0
-10

**Figure 3**

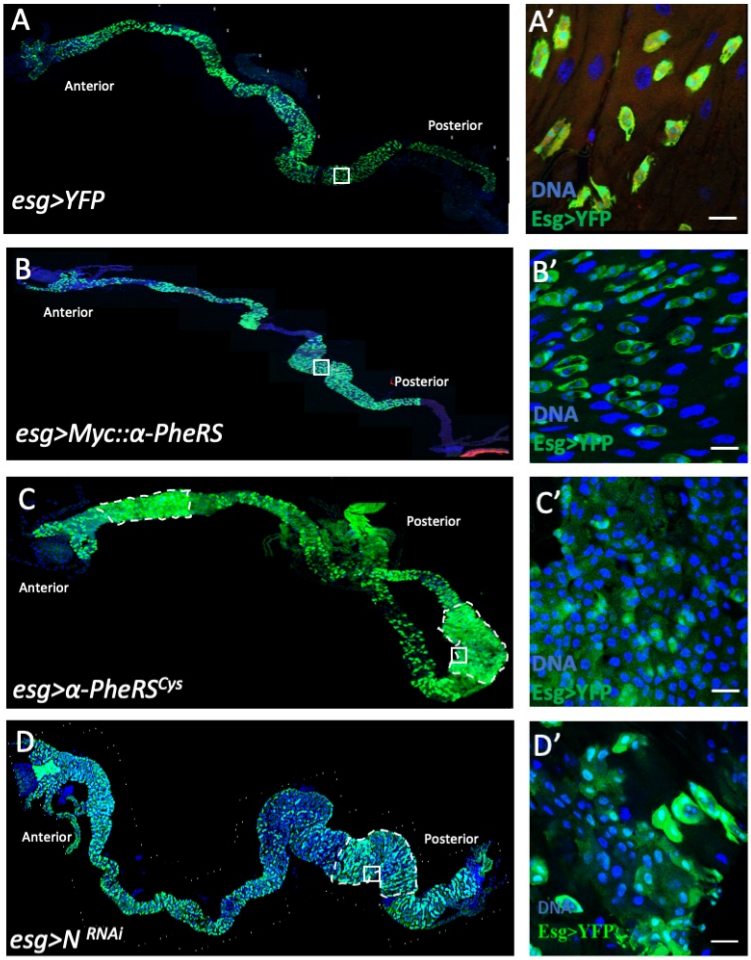
A
Anterior
Posterior
esg>YFP
A'
DNA
Esg>YFP
B
Anterior
Posterior
esg>Myc::α-PheRS
B'
DNA
Esg>YFP
C
Anterior
Posterior
esg>α-PheRSCys
C'
DNA
Esg>YFP
D
Anterior
Posterior
esg>N RNAi
D'
DNA
Esg>YFP

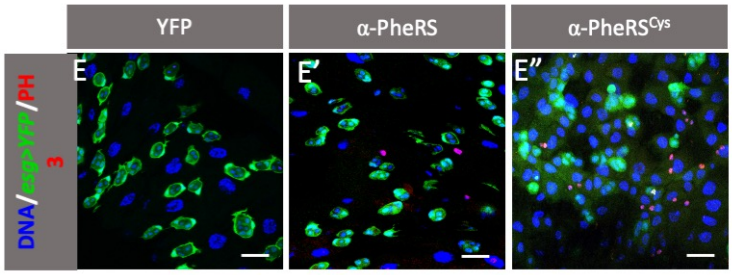
YFP
α-PheRS
α-PheRSCys
DNA/esg>YFP/PH3
E
E'
E''

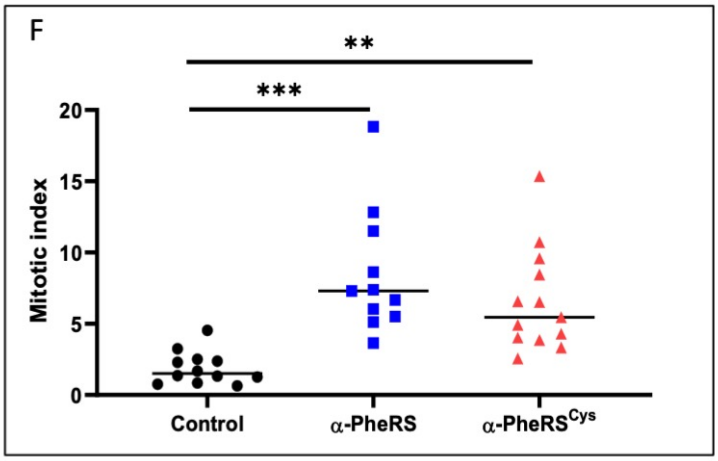
F
**
***
Mitotic index
20
15
10
5
0
Control
α-PheRS
α-PheRSCys

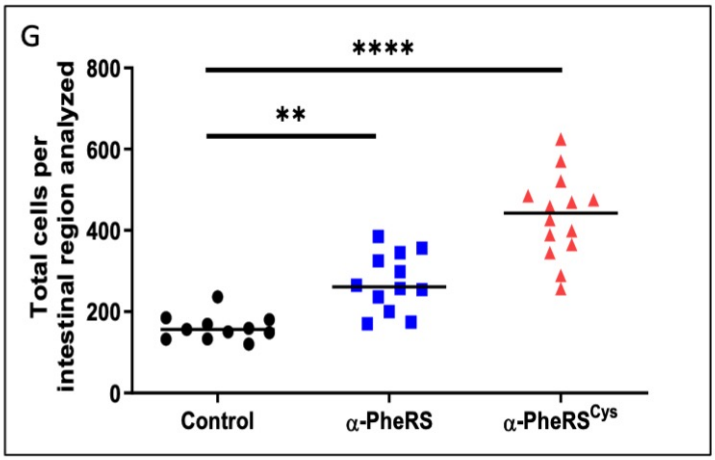
G
****
**
Total cells per intestinal region analyzed
800
600
400
200
0
Control
α-PheRS
α-PheRSCys

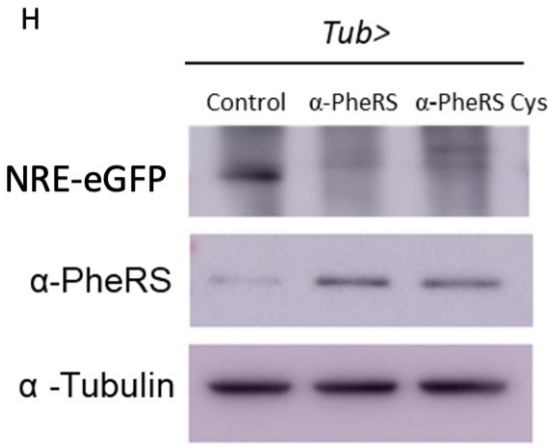
H
Tub>
Control
α-PheRS
α-PheRS Cys
NRE-eGFP
α-PheRS
α -Tubulin

**Figure 4**

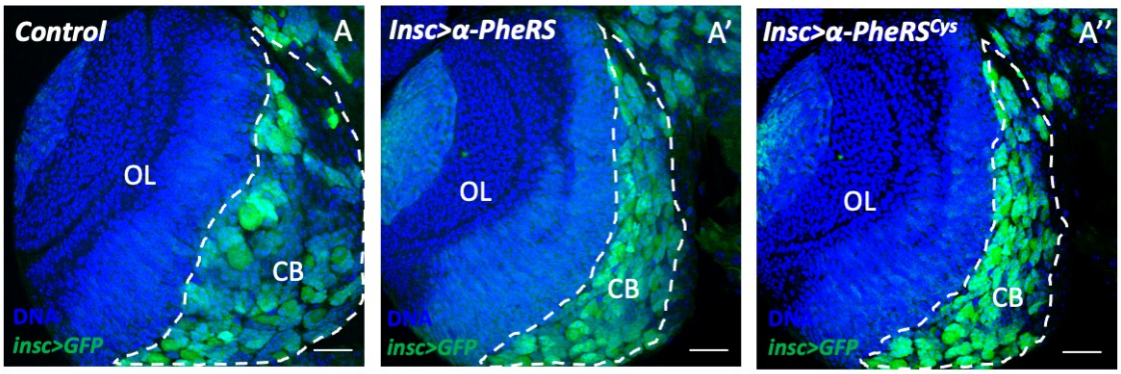
Control
A
OL
CB
DNA
insc>GFP
Insc>α-PheRS
A'
OL
CB
DNA
insc>GFP
Insc>α-PheRS^Cys
A''
OL
CB
DNA
insc>GFP

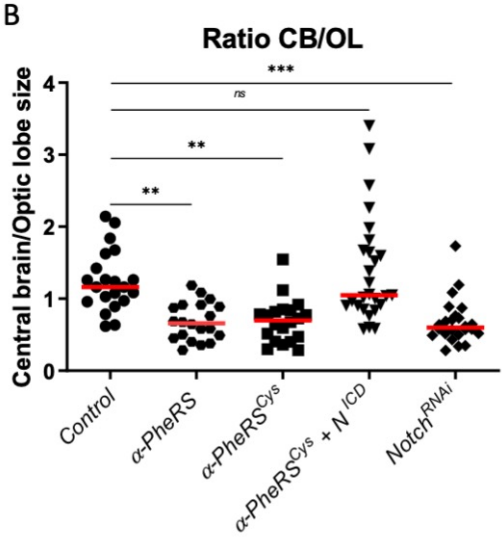
B
Ratio CB/OL
Central brain/Optic lobe size
0
1
2
3
4
***
ns
**
**
Control
α-PheRS
α-PheRS^Cys
α-PheRS^Cys + N^ICD
Notch^RNAi

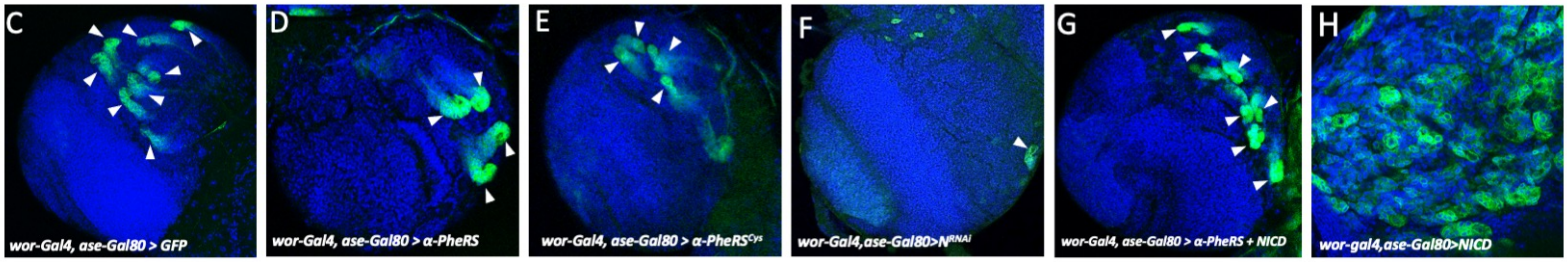
C
wor-Gal4, ase-Gal80 > GFP
D
wor-Gal4, ase-Gal80 > α-PheRS
E
wor-Gal4, ase-Gal80 > α-PheRS^Cys
F
wor-Gal4,ase-Gal80>N^RNAi
G
wor-Gal4, ase-Gal80 > α-PheRS + NICD
H
wor-gal4,ase-Gal80>NICD

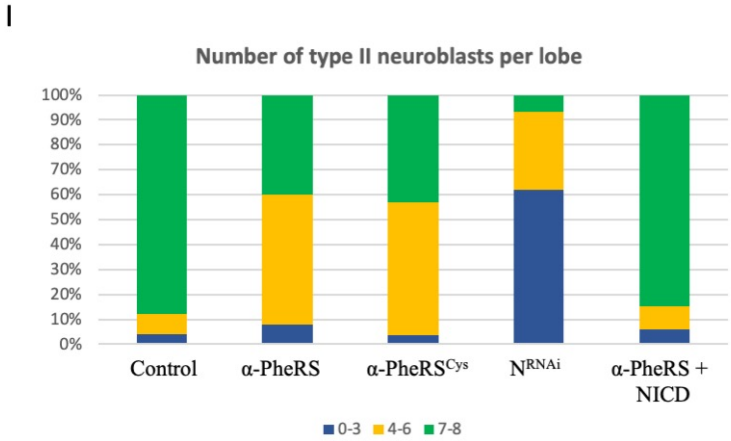
I
Number of type II neuroblasts per lobe
100%
90%
80%
70%
60%
50%
40%
30%
20%
10%
0%
Control
α-PheRS
α-PheRS^Cys
N^RNAi
α-PheRS + NICD
0-3
4-6
7-8

**Figure 5**

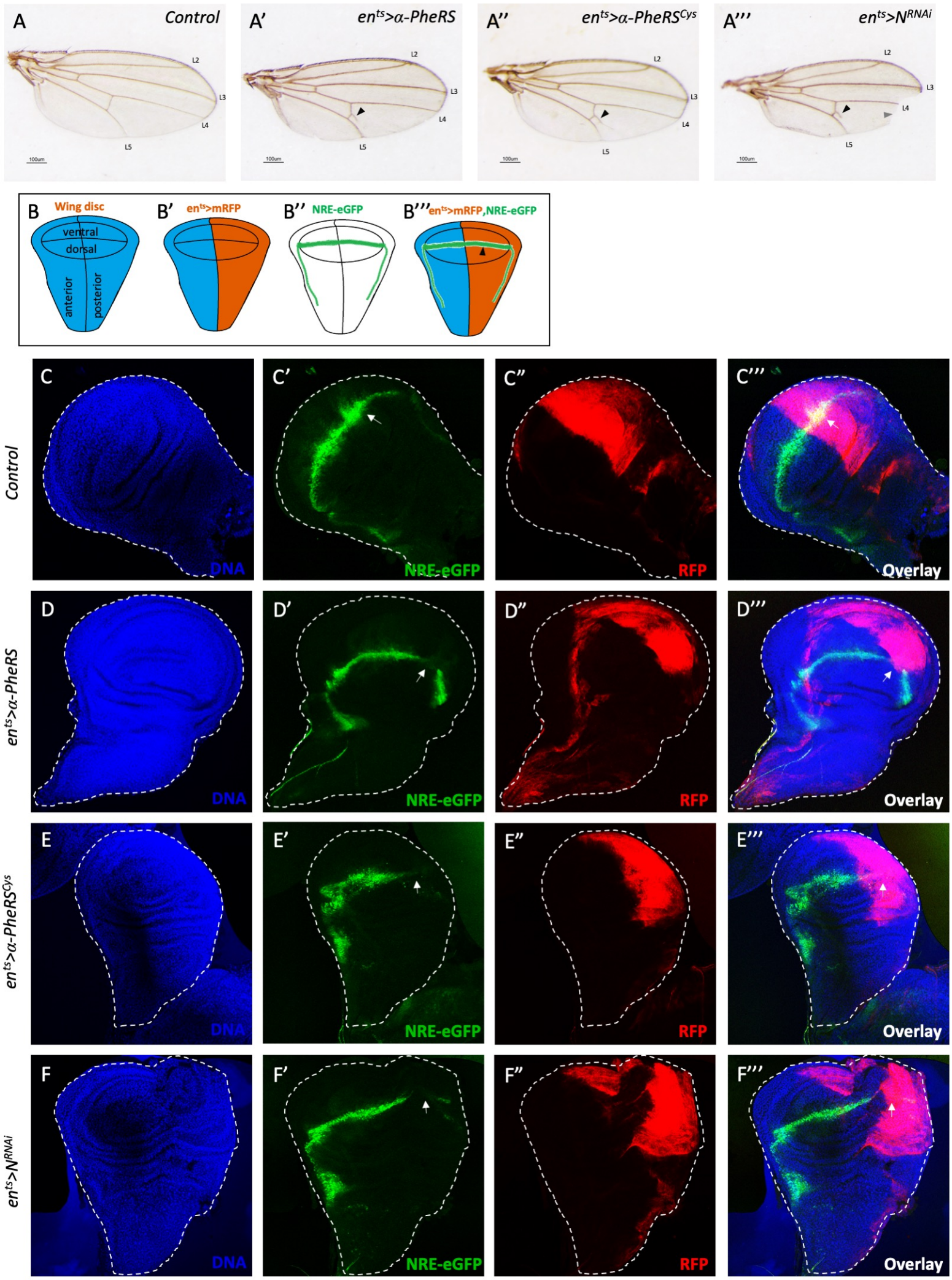
A
Control
A'
en^ts>α-PheRS
A''
en^ts>α-PheRS^Cys
A'''
en^ts>N^RNAi
L2
L3
L4
L5
100um
B
Wing disc
ventral
dorsal
anterior
posterior
B'
en^ts>mRFP
B''
NRE-eGFP
B'''
en^ts>mRFP,NRE-eGFP
Control
en^ts>α-PheRS
en^ts>α-PheRS^Cys
en^ts>N^RNAi
C
C'
C''
C'''
D
D'
D''
D'''
E
E'
E''
E'''
F
F'
F''
F'''
DNA
NRE-eGFP
RFP
Overlay

**Figure 6**

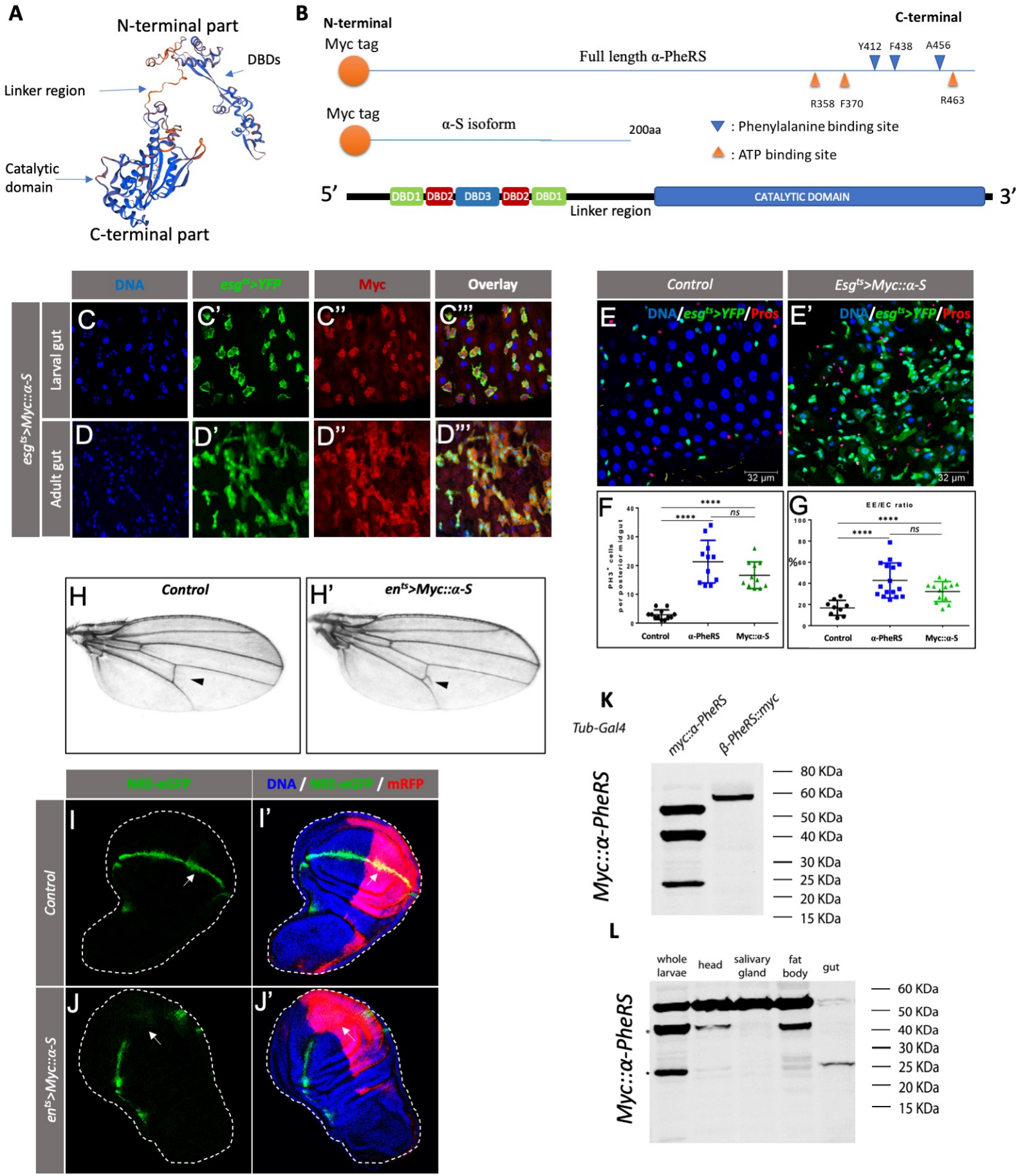
A
N-terminal part
DBDs
Linker region
Catalytic domain
C-terminal part
B
N-terminal
Myc tag
Full length α-PheRS
C-terminal
Y412 F438 A456
R358 F370
R463
Myc tag
α-S isoform
200aa
: Phenylalanine binding site
: ATP binding site
5'
DBD1 DBD2 DBD3 DBD2 DBD1
Linker region
CATALYTIC DOMAIN
3'
DNA
esg^ts>YFP
Myc
Overlay
esg^ts>Myc::α-S
Larval gut
Adult gut
C
C'
C''
C'''
D
D'
D''
D'''
Control
Esg^ts>Myc::α-S
E
DNA/esg^ts>YFP/Pros
E'
32 µm
F
PH3+ cells per posterior midgut
Control
α-PheRS
Myc::α-S
G
EE/EC ratio
%
H
Control
H'
en^ts>Myc::α-S
NRE-eGFP
DNA / NRE-eGFP / mRFP
I
I'
J
J'
K
Tub-Gal4
myc::α-PheRS
β-PheRS::myc
Myc::α-PheRS
80 KDa
60 KDa
50 KDa
40 KDa
30 KDa
25 KDa
20 KDa
15 KDa
L
whole larvae
head
salivary gland
fat body
gut
Myc::α-PheRS
60 KDa
50 KDa
40 KDa
30 KDa
25 KDa
20 KDa
15 KDa

**Figure 7**

**A**

## Alignment of Notch and α-S polypeptide sequence
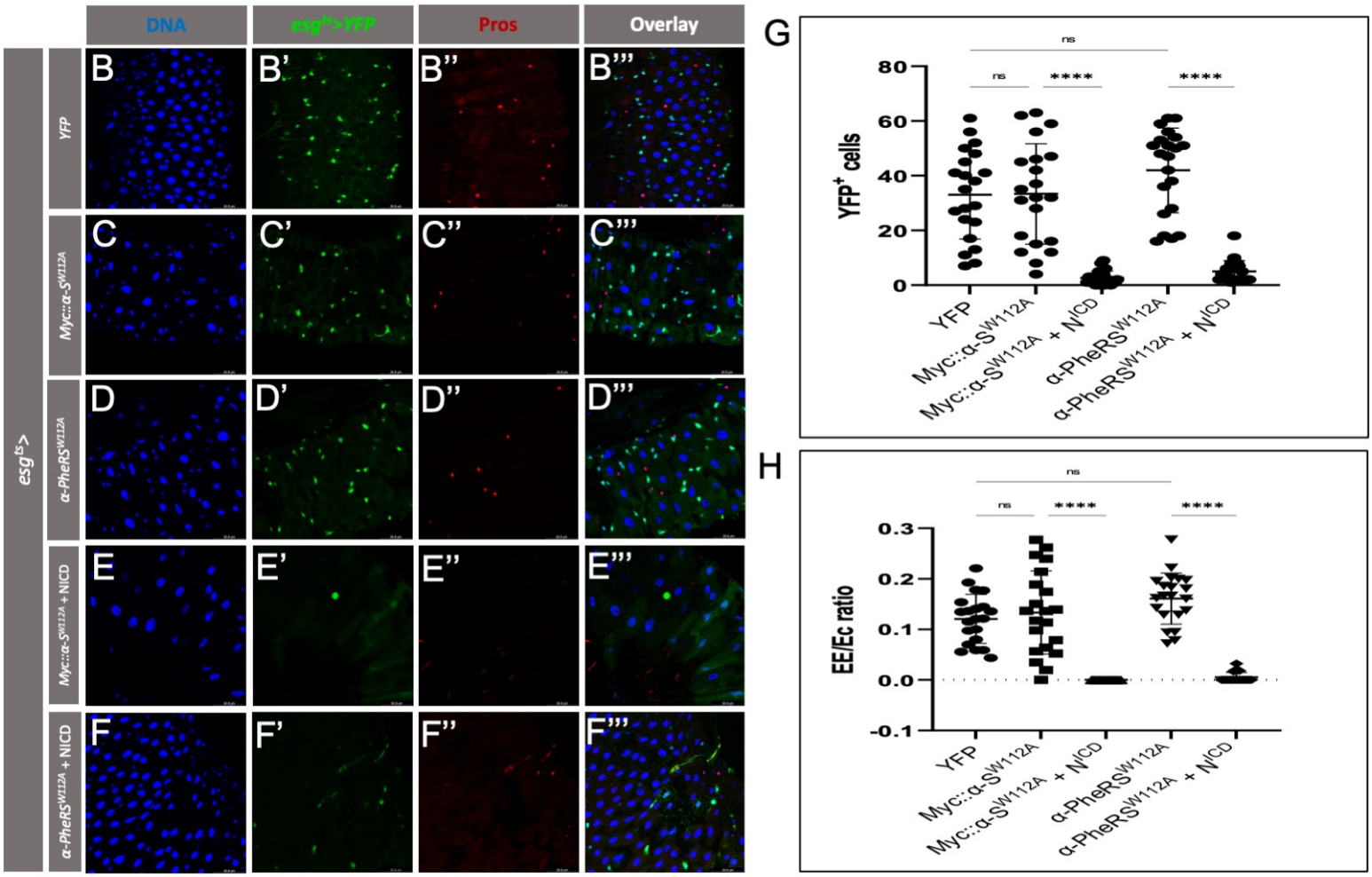
```
P07207 NOTCH_DROME      1681  GIQIYLEIDNRKCTECFTHAVEAAEFLAATAAKHQLRNDFQIHSVRGIKNPGDE--DNGE      1738
Q9W3J5 SYFA_DROME         25  --AALFAEDHQKIVGSLKSIQAHGELVTAE---------TVTHKSLGLTDEGRAVVENGS        73
                                   :  *::* . .:.     .*:::*              *.  *:.: *    :**.
                                                                  RAM
P07207 NOTCH_DROME      1739  PPANVKYVI--TGIILVIIALAFFGMVLSTQRKRAHGVTWFPEGFRAPAAVMSRRRRDPH      1796
Q9W3J5 SYFA_DROME         74  HEALVYDLVPPEGIAQAA-LMAAGGANAKVGFSKAMSHGWILVDKSVTPP-LVRRKVDTI       131
                                * *  ::   **  .   :*  *   ..  .:* .  *:  .  .    : **: *
                                                  RAM
P07207 NOTCH_DROME      1797  GQEMRNLNKQVAMQSQGVGQPGAHWSDDESDMPLPKRQRSDPVSGVGLGNNGGYASDHTM      1856
Q9W3J5 SYFA_DROME        132  TDVVRNQLQQVALGK-GDQLPAKEVAD----FKKRKLLQETTTKSFVLARGPEFATTLTK       186
                                : :**  :***: . *   *. . :*    :   *  :.  .... *...  :*:  *
                                                  RAM
P07207 NOTCH_DROME      1857  ---VSEYEEADQRVWSQAHLDVVDVRAIMTPPAHQDGGKHDVDARGPCGLTPLMIAAVRG      1913
Q9W3J5 SYFA_DROME        187  LETDLTVEMLANGLWDQLKFKAYNFDALGAPPTRGH-------------LHPLLK-----       228
                                     *   : :*.* ::.. :. *: :**:: .             * **:
```